This volume is the property of the University of Oklahoma, but the literary rights of the author are a separate property and must be respected. Passages must not be copied or closely paraphrased without the previous written consent of the author. If the reader obtains any assistance from this volume, he must give proper credit in his own work.

I grant the University of Oklahoma Libraries permission to make a copy of my thesis upon the request of individuals or libraries. This permission is granted with the understanding that a copy will be provided for research purposes only, and that requestors will be informed of these restrictions.

NAME [redacted]

DATE [redacted]

A library which borrows this thesis for use by its patrons is expected to secure the signature of each user.

This thesis by ARISTOTELIS PAGOULATOS has been used by the following persons, whose signatures attest their acceptance of the above restrictions.

| NAME AND ADDRESS | DATE |
|---|---|

OU-138

Downloaded from SHAREOK. Persistent Handle URL: https://hdl.handle.net/11244/323808

THE UNIVERSITY OF OKLAHOMA

GRADUATE COLLEGE

# EVALUATION OF MULTISTAGE TRIAXIAL TESTING ON BEREA SANDSTONE

A THESIS SUBMITTED TO THE GRADUATE FACULTY

in partial fulfilment of the requirements for the

DEGREE OF

MASTER OF SCIENCE

BY

ARISTOTELIS PAGOULATOS

NORMAN, OKLAHOMA

2004

UNIVERSITY OF OKLAHOMA
LIBRARIES

# EVALUATION OF MULTISTAGE TRIAXIAL TESTING ON BEREA SANDSTONE

A THESIS APPROVED FOR THE

MEWBOURNE SCHOOL OF PETROLEUM AND GEOLOGICAL ENGINEERING

BY

Chair: [redacted]

Carl Sondergeld, PhD.

Member: [redacted]

Chandra Raj, PhD.

Member: [redacted]

Subhash Shah, PhD.

©Copyright Athanasia Papoulatos, 2004

All rights reserved

©Copyright Aristotelis Pagoulatos, 2004

All rights reserved

*To my family that gave me everything,*
*but mostly they gave me the luxury*
*to plan my own future.*

## Acknowledgments

I would like to thank Dr. Carl Sondergeld for being my advisor and helping me all these years with corrections that were aiming to my excellence not only as a student but also as a scientist. I admire his passion for perfection and his effort for transmitting his knowledge to others. Dr. Carl, I so appreciate your time and your efforts.

Dr. Chandra Rai was the person that had a solution for all the problems and it was he that I had to count on the numerous problems while studying here. With advises on my papers and on my life too, he would make me leave his office with a nice optimistic feeling each time.

I would like to thank Subhash Shah for being in my thesis committee and for his valuable suggestions and comments on my thesis.

The $IC^3$ lab is always going to be a nice memory and an incredible experience as my life goes on. Gary Stowe and Bruce Spears were very friendly and helpful making my staying pleasant and productive. I want to thank them not only for their excellent lab assistance but for being the people I wanted to see everyday and work with.

I want to thank Dr. J. C. Roegiers for the entire knowledge and the good *off campus* times we had together. He is the person whose connections open doors for my career and he didn't hesitate a moment to provide me any help I would have asked.

Finally, I would like Michelle for her unconditional love. She was my greatest inspiration and there are no words to thank her for that.

## TABLE OF CONTENTS


**ABSTRACT** ..... **XII**

**CHAPTER 1** ..... **1**

1.1 STATEMENT OF THE PROBLEM ..... 1
1.2 OVERVIEW ..... 3

**CHAPTER 2** ..... **10**

2.1 MECHANICAL PROPERTIES ..... 10
*2.1.1 Strength* ..... *11*
*2.1.2 Young's Modulus, E* ..... *11*
*2.1.3 Poisson's ratio, v* ..... *12*
*2.1.4 Dynamic moduli* ..... *12*
*2.1.5 Mohr's plot, failure envelope, angle of friction and cohesive strength.* ..... *13*
2.2 EVALUATION OF TESTING AND CAPABILITIES ..... 16
*2.2.1 Uniaxial test* ..... *16*
*2.2.2 Triaxial test* ..... *17*
*2.2.3 Polyaxial test* ..... *19*
*2.2.4 Multistage technique* ..... *19*
2.3 VOLUMETRIC STRAIN AS A MONITORING PARAMETER ..... 20
2.4 RHEOLOGICAL CONSIDERATIONS. BRITTLE-DUCTILE TRANSITION ..... 25

**CHAPTER 3** ..... **30**

3.1 SAMPLE CHARACTERIZATION ..... 30
*3.1.1 Porosity* ..... *30*
*3.1.2 Permeability* ..... *31*
*3.1.3 Mineralogy* ..... *32*
*3.1.4 Photographs of failed samples* ..... *33*
*3.1.5 Velocities* ..... *34*
3.2 CHARACTERIZATION SUMMARY ..... 34
*3.2.1 Porosity* ..... *35*
*3.2.2 Permeability* ..... *36*
*3.2.3 Velocities* ..... *39*
*3.2.4 Sample preparation* ..... *41*

**CHAPTER 4** ..... **46**

4.1 MULTISTAGE METHODS; A REVIEW ..... 46
*4.1.1 Literature review* ..... *46*
*4.1.2 The "sign of failure" criterion* ..... *46*
*4.1.3 Using the volumetric strain* ..... *51*
*4.1.4 Drawbacks to previous approaches* ..... *54*

**CHAPTER 5** ..... **57**

5.1 THE PROPOSED METHOD ..... 57
*5.1.1 Introduction* ..... *57*
*5.1.2 Methodology* ..... *58*
*5.1.3 Construction of the failure envelope* ..... *70*
*5.1.4 Data Analysis* ..... *73*

**CHAPTER 6** ..... **87**

6.1 SUMMARY ..... 87
6.2 CONCLUSIONS ..... 91

**NOMENCLATURE** ..... **92**

**REFERENCES** ..... **93**

**APPENDIX I** ..... **97**

STRESS-STRAIN PLOTS OF SINGLE STAGE TESTS ..... 97

**APPENDIX II** ..... **106**

STRESS-STRAIN PLOTS OF MULTISTAGE TESTS ..... 106

**APPENDIX III** ..... **109**

EXAMINATION OF STRESS DIFFERENCE DEPENDENCY UPON MEASURED PHYSICAL PARAMETERS AND MINERALOGY ..... 109

**APPENDIX IV** ..... **113**

PHOTOGRAPHS OF THE FAILED SAMPLES ..... 113

## LIST OF TABLES

Table 3.1 Mineralogical composition of 15 Berea sandstone samples ..... 38
Table 3.2 Compressional (P) and shear ($S_1$-$S_2$) waves reported as a function of confining pressures ..... 40
Table 5.1 Single stage triaxial test results ..... 62
Table 5.2 Data obtained from single stage tests for various confining pressures. 65
Table 5.3 Failure stresses obtained from single stage tests for various confining pressures. ..... 74
Table 5.4 Summary of reported mechanical data results for Berea sandstone. .... 75
Table 5.5 Failure envelope data obtained from conventional single stage and multistage methods ..... 77
Table 5.6 Changes of Young's modulus and Poisson's ratio, for a sample after six cycles of loading and unloading to the deflection point ..... 81
Table 5.7 Summary of the mechanical properties obtained from single stage tests. ..... 84
Table 5.8 Summary of the mechanical properties obtained from multistage stage tests of sample H1. ..... 84
Table 5.9 Summary of single stage tests. ..... 85
Table 5.10 Summary of mechanical properties of multistage tests. ..... 86
Table 6.1 Summary of failure envelope parameters derived from the present multistage technique and those from single stage tests. ..... 89

## LIST OF FIGURES

Figure 2.1 Failure modes and stresses for (a) brittle and (b) ductile materials..... 11
Figure 2.2 Sketch of the Mohr's failure envelope and the Mohr's Coulomb failure criterion (Hudson and Harrison, 1997). ..... 15
Figure 3.1 Automated porosimeter apparatus ..... 31
Figure 3.2 CMS apparatus in the $IC^3$ ..... 32
Figure 3.3 FTIR apparatus in the $IC^3$ laboratory.. ..... 33
Figure 3.4 Photograph, showing the original block ..... 35
Figure 3.5 Porosity as a function of confining pressure.. ..... 36
Figure 3.6 Klinkenberg correct permeabilities as a function of confining pressure. ..... 37
Figure 3.7 Average mineral composition ..... 38
Figure 3.8 Stress distribution for a uniaxial test. (Hawkes and Mellor, 1970). ..... 42
Figure 3.9 Preparation of the sample ..... 43
Figure 3.10 The lateral extensometer mounted on the sample. ..... 44
Figure 3.11 Both lateral and axial extensometers mounted on the sample..... 45
Figure 4.1 Results of multistage (M.S.) and single stage (S.S.) triaxial tests for Lyons sandstone by Kim and Ko (1979). ..... 49
Figure 4.2 Stress paths followed in tests by Kovari et al. (1983). ..... 50
Figure 4.3 Construction of the failure envelope using the method proposed by Kovari et al. (1983). ..... 51
Figure 4.4 Comparison between multistage and single stage triaxial test results (Crawford and Wylie, 1987) ..... 52
Figure 4.5 Multistage testing (Bro, 1995)..... 53
Figure 4.6 Strain dependencies of Bro's results for the angle of friction and cohesion (Bro, 1995)..... 54
Figure 5.1 Applied axial stress versus strains for sample H8. ..... 59
Figure 5.2 Confining pressure dependency of the pressure difference between the stresses at the point where the volumetric strain is equal to zero and the failure stress ..... 59
Figure 5.3 Typical stress strain plot of Berea (17.2 MPa confining pressure) where the deflection point of the volumetric strain is indicated..... 61
Figure 5.4 Pressure dependence of the stress difference between the failure and the deflection of the volumetric strain. ..... 62
Figure 5.5 Plot of the shear failure stress for different confining pressures and the line that separates brittle and ductile behavior (Byerlee, 1968)..... 64
Figure 5.6 Comparison between failure envelopes obtained from the three stress termination criteria (1) stress at failure, (2) stress when the volumetric strain is equal to zero and (3) deflection point of the volumetric strain. ..... 66

Figure 5.7 Complete stress path for a multistage test in q-p space. ..... 69
Figure 5.8 Complete multistage test for sample H26. ..... 69
Figure 5.9a Final failure envelope obtained from multistage tests ..... 72
Figure 5.10 Complete multistage test ..... 76
Figure 5.11 Failure envelope data obtained from conventional single stage and multistage methods for sample H26 ..... 77
Figure 5.12 Summary of multistage results for four samples of Berea sandstone. ..... 78
Figure 5.13 Comparison between static, E, and dynamic Young's moduli, $E_D$. .. 79
Figure 5.14 Young's modulus measured from conventional and multistage tests. ..... 80
Figure 5.15 Stress-strain plot showing the axial the lateral and the volumetric strains of the cycled sample H20. ..... 82
Figure 5.16 Sample broken at 17.24 MPa. The red line is the number of acoustic emissions divided by 20,000. ..... 83
Figure AI.1 Sample H20 tested uniaxially. ..... 98
Figure AI.2 Sample H21 tested triaxially at 3.45 MPa confining pressure. ..... 99
Figure AI.3 Sample H24 tested triaxially at 6.8 MPa confining pressure. ..... 100
Figure AI.4 Sample H5 tested triaxially at 17.24 MPa confining pressure. ..... 101
Figure AI.5 Sample H9 tested triaxially at 24.14 MPa confining pressure. ..... 102
Figure AI.6 Sample H21 tested triaxially at 34.48 MPa confining pressure. ..... 103
Figure AI.7 Sample H27 tested triaxially at 41.4 MPa confining pressure. ..... 104
Figure AI.8 Sample H8 tested triaxially at 55.17 MPa confining pressure. ..... 105
Figure AII.1 Sample H1 tested using multistage triaxial technique. ..... 107
Figure AII.2 Sample H26 tested using multistage triaxial technique. ..... 108
Figure AIII.1 Stress difference between failure stress and stress at the deflection of the volumetric strain plotted against the percentage of total clay content. ..... 110
Figure AIII.2 Stress difference between failure stress and stress at the deflection of the volumetric strain plotted against the Young's modulus. ..... 110
Figure AIII.3 Stress difference between failure stress and stress at the deflection of the volumetric strain plotted against porosity ..... 111
Figure AIII.4 Stress difference between failure stress and stress at the deflection of the volumetric strain plotted against permeability. ..... 111
Figure AIII.5 Permeability plotted against percentage of clay minerals. ..... 112
Figure AIII.6 Plot of reported mechanical data results for Berea sandstone. ..... 112
Figure AIV.1 Photograph of a multistage sample H16 after the completion of the test. (Porosity = 19.4%; k = 148 mD; $\beta = 60^{o}$). ..... 114
Figure AIV.2 Photograph showing the failure plane orientation for multistage sample 22. (Porosity = 18.6%; k = 101 mD; $\beta = 62^{o}$). ..... 114

Figure AIV.3 Photograph of sample H23 ($\sigma_c$ = 17.24; $\sigma_f$ = 172 MPa Porosity = 22%; k = 110 mD; $\beta = 65^o$)..... 115
Figure AIV.4 Photograph of multistage sample H26 (Porosity = 19.1%; k = 200 mD; $\beta = 60^o$). ..... 115
Figure AIV.5 Photograph of sample H8 ($\sigma_c$ = 55.17; $\sigma_f$ = 281 MPa Porosity = 19.5%; k = 174 mD; $\beta = 55^o$)..... 116
Figure AIV.6 Photograph of sample H13 showing ductile failure. ($\sigma_c$ = 3.45MPa; $\sigma_f$ = 95.9 MPa Porosity = 19.1%; k = 150 mD; $\beta \approx 90^o$)..... 116
Figure AIV.7 Photograph of sample H3 ($\sigma_c$ = 3.45MPa; $\sigma_f$ = 95.9 MPa Porosity = 19.1%; k = 150 mD; $\beta \approx 90^o$)..... 117

## Abstract

Conventional methods for obtaining failure envelopes require testing multiple samples, a luxury not enjoyed when dealing with core recovered from boreholes. Consequently, a multistage test performed on a single plug is attractive not only because it requires a single sample but it is both less expensive and requires less time. It has another major advantage in minimizing sample heterogeneity. Previous studies using multistage triaxial tests indicate that they can be an efficient approach to determining mechanical properties. However, critical to the recovery of meaningful data is the definition of the stress cycle termination point. We propose a new approach to defining the termination point.

In this study, plugs from a common block of Berea sandstone were tested using both conventional and multistage triaxial testing methods. In our multistage tests we evaluated the inflection point of the volumetric strain curve i.e., when the derivative of the volumetric strain is equal to zero, as a termination point. The values of Young's modulus, E and Poisson's ratio, $\nu$, and the failure envelope characteristics show better agreement with those derived from single-stage conventional tests when the new termination criterion is used.

# Chapter 1

## *1.1 Statement of the problem*

This thesis addresses the optimization of mechanical properties measurements (E, $\nu$, $\sigma_f$) on rock under the constraint of limited availability.

Analysis of wellbore stability, sand production, hydraulic fracturing and reserve estimation require measurements of physical properties such as failure strength ($\sigma_f$), failure envelope characteristics (C, $\phi$), compressibility (c), Young's modulus (E) Poisson's ratio ($\nu$), etc. Acquiring this information is costly and time consuming. As a result, these considerations force engineers to make assumptions rather than making measurements. This leads to wrong predictions. Consequently, any effort towards reducing either the cost of obtaining this information, or the time required, are economically attractive to engineers.

To put the additional cost of measurement in perspective, we consider the cost of obtaining core. The cost of extracting the plug from its *in situ* position, under specific conditions like offshore platforms, may be about $10,000 per foot of core. The cost of the laboratory tests vary from $25 for simple porosity and permeability to $1500 for complicated mechanical tests. Consider that at most three mechanical test plugs can be taken from one foot of core, the additional measurement cost about $4500/ft. Since one foot of core can represent millions of

years in geologic time, individual plugs can display substantial heterogeneity, reflecting changes in sedimentation over that time period.

These considerations become more critical when calculating properties like angle of friction and cohesion where according to the conventional methods, tests on more than one plug are required for the estimation of these values. In this case if fewer samples could be used for the calculations, the influence of sample heterogeneity could be reduced and the cost could be reduced. To solve this problem presented by cost and limited core, scientists proposed a multistage triaxial technique of testing rock (Crawford and Wylie, 1987; Kim and Ko, 1979; Kovari et al., 1983; Harouaka et al., 1995).

Multistage is a method in which testing a single plug under more than one confining pressures can yield the equivalent results of testing multiple plugs under different confining pressures. The test consists of multiple loading stages and each stage is terminated before failure. The confining pressure is increased and the same procedure is repeated for as many confining pressures as required. However, the existing multistage methods are complex and they result in failure envelope characteristics that represent a much weaker rock compared to the respective values obtained by conventional methods.

In this thesis a new method of performing multistage triaxial tests is proposed. All mechanical properties of rock for various confining pressures can be derived from a single plug. The advantages of my method over previously

suggested methods are that it is very easy to perform and the results are quite reproducible and comparable with conventional results. Additionally it guarantees the integrity of the plug until the end of the test. The cost of acquiring the data from a formation is reduced considerably and the additional core, if existing, can be used to increase the confidence in the results statistically.

## 1.2 Overview

Conventional methods for obtaining failure envelopes require testing on multiple core samples, a luxury not enjoyed when dealing with core of limited diameter from boreholes. Consequently, a multistage test requiring a single plug is attractive because it is both less expensive and less time consuming. It has another major advantage in eliminating sample to sample heterogeneity. Previous studies using multistage triaxial tests (Kovari and Tisa, 1975) indicate that it can be an efficient approach to determining mechanical properties. However, critical to the recovery of meaningful data is the definition of the stress cycle termination point. Our effort focuses on defining this termination point.

In this study, plugs from a common block of Berea sandstone were tested using both conventional and multistage triaxial testing methods. In our multistage tests we use the inflection point of the volumetric strain curve i.e., when the derivative of the volumetric strain is equal to zero, as a termination point. The failure envelope characteristics (cohesion and angle of internal friction) and the

values of Young's modulus (E) and Poisson's ratio (ν) obtained from multistage test are compared to those obtained from single stage conventional test.

The first description of multistage mechanical tests was given by Kovari and Tisa (1975). They suggested stopping the triaxial test at the point before the sample exhibits signs of approaching failure. However, Kim and Ko (1979) describe the dependency of the effectiveness of this method on the type of stress – strain curve. Kim and Ko (1979) report that the quality of the results strongly depends on the post failure behavior of the rock. Subsequently, Crawford and Wylie, (1987), defined the termination point to be when the volumetric strain reaches zero. Both methods suffer from the following drawbacks: 1) the sample can fail prior to the end the loading cycle and 2) the results depend critically on the subjectivity of the experimenter in defining the termination point and can therefore be inconsistent between laboratories.

In this paper a different approach to performing the multistage triaxial test is proposed. The points at which stages within the test are ceased are easy to pick and guarantee the integrity of the sample. Furthermore the plug experiences minimum alteration of its mechanical properties, as it is never stressed much beyond the elastic region. The data acquired from this new method can be used to construct a complete failure envelope from a single sample.

**Sample preparation and characterization**

One and a half inch (3.81 cm) diameter samples were cored vertically with respect to the bedding. A length to diameter ratio of 2:1 was maintained. The two ends were polished flat and parallel in accordance with the ASTM guidelines (1980) for triaxial testing. The samples were cleaned in a Soxhlet extractor and dried in a vacuum oven at 100 $^{o}$C. Tests were performed under ambient temperature and humidity conditions. Samples were jacketed in polyolefin heat shrink tubing and sealed to endcaps with twisted wire.

In an effort to minimize heterogeneity effects and identify the sources that may cause changes in the rock strength, extensive sample characterization was performed. This characterization was used to assess the homogeneity of samples taken from the same block of Berea. Part of this characterization process included determining the mineralogical composition through an FTIR transmission technique (Sondergeld and Rai, 1993). Little variability among the tested samples was found. In addition, porosity and permeability were measured as a function of confining pressure. Compressional and shear wave velocities were also measured as a function of confining pressure in separate tests.

**Multistage techniques**

In an effort to optimize the multistage testing procedure, various criteria for determining the stage termination point have been evaluated. The termination

stress most widely used by researchers is that of "a sample exhibiting failure". However, there is no doubt irreversible mechanical changes take place in the samples experiencing these stress magnitudes.

In this study, the inflection point on the volumetric strain ($\varepsilon_{vol.}$) curve was used as the termination point. This point represents the transition from stable crack propagation to unstable crack propagation (Bieniawski, 1967) and is selected to avoid partial or total failure of the specimen. The inflection point is defined as the point where the volumetric strain curve starts decreasing after peaking and the derivative of the curve at that point is equal to zero ($\frac{d\varepsilon_{vol.}}{d\sigma} = 0$). The inflection point of the volumetric strain is the point where more cracks are being created than closed. Based on my observations from single stage tests, this point is related to failure and it has a uniform deviation from the failure point.

We can construct a failure envelope based on the stresses at the inflection points which will be shown to be parallel to the one constructed from failure stresses. This is a result of the consistency of the difference in stresses between the failure point and the inflection point for all the confining pressures below 34.5 MPa. This information can be obtained before reaching the strength limit of the sample so there is no need to know *a priori* the behavior of the failure curve to have meaningful results.

**Construction of failure envelope**

Failure stresses and confining pressures are required to construct the Mohr's stress circles and failure envelope. The failure envelope is defined to be the common tangent to all the Mohr's failure circles. The slope of the failure envelope represents the tangent of the angle, $\phi$, of the failure plane of the sample, and the intersection with the ordinate yields the cohesive strength, **C**, of the rock (Jaeger and Cook, 1979).

However, in multistage tests following the procedure described above, the stress obtained from each pressure stage is the stress at the inflection point of the volumetric strain curve and not the failure stress. Note though that the sample is brought to failure on the last pressure stage; this yields both stress at failure and at the maximum inflection point. The cumulative data collected on each multistage test consists of numerous inflection point stresses, Young's moduli, Poisson's ratios and one failure strength from the last stage.

The failure envelope constructed from the stresses obtained from the inflection points is essentially parallel to the failure envelope obtained using the failure stresses from conventional tests. In contrast, the failure envelope defined from the values where the volumetric strain is equal to zero is not.

After drawing the failure envelope based on stresses at the inflection points, we shift this initial failure envelope so that it becomes tangent to the second circle made using the failure stress from the terminal cycle. The shifted

failure envelope produced by the multistage test is then comparable to the failure envelope obtained by the conventional testing method.

The behavior of the volumetric strain is very repeatable and appears to be a safe criterion for terminating test stages. The difference between the inflection point and the failure point is observed to be nearly constant and more importantly it appears not to be confining pressure dependent, in contrast to the behavior of the point defined where $\varepsilon_{vol}=0$. The point where $\varepsilon_{vol}=0$ is strongly pressure dependent, having larger values at low confining pressures. Furthermore, after a number of tests no sample broke or showed any signs of failure earlier than the inflection point of its volumetric strain. However, some samples at high confining pressures, did fail before the volumetric strain approached the zero value. The results of the multistage tests were compared to single-stage tests and the agreement was very good.

The Young's moduli, **E**, obtained from the multistage tests yield the expected trend when plotted against the confining pressure; **E** increased as the confining pressure increased. In contrast, the trend obtained by using the conventional testing method does not follow the expected trend due to the initial sample heterogeneity. Finally, the comparison of static with dynamic data, derived from the measured velocities and densities, is poor at low confining pressures and quite good at higher confining pressures. This suggests the differences between dynamic and static moduli are largely driven by cracks.

Cracks cause nonlinear behavior (Guyer and Johnson, 1999) in rocks rendering direct comparisons between static and dynamic properties meaningless.

# Chapter 2

## 2.1 Mechanical properties

Ultimate strength, Young's modulus, Poisson's ratio, failure envelope, angle of internal friction and cohesive strength are some of the most commonly required mechanical properties. These properties are used to predict the behavior of rock when subjected to stress such as in formation subsidence, borehole stability and sanding or hydraulic fracturing.

Triaxial tests are the mechanical tests in which these properties are measured. Samples, precisely machined core plugs, are mounted inside a pressure vessel and instrumented to measure the axial and lateral strains. Triaxial tests are performed by first applying confining pressure, $\sigma_c$, and then increasing axial load. Uniaxial tests differ in that the confining pressure is zero. Both tests can be carried out to specimen failure. During the test, the applied stresses and the resulting strains are monitored. Strain is defined as the change of the length caused by applied stress over the initial length. The strain that has the same direction as the applied compressional stress ($\sigma_1$) is called axial strain ($\varepsilon_a$) and the strain orthogonal to the axial is called lateral strain ($\varepsilon_L$). Assuming that strains are infinitesimals, the summation of all three strains (one axial and two laterals) gives the volumetric strain ($\varepsilon_{vol}$), to first order. The volumetric strain as the name suggests describes the change in sample volume.

### 2.1.1 Strength

One of the most valuable and often required properties of rock is strength, $\sigma_f$. The direct method of measuring $\sigma_f$ is by performing a uniaxial test and recording the maximum supported load before failure and losing consistency (Figure 2.1a). This applies for brittle failure. The strength of a ductile material strength is considered to be the stress above which the rock shows a large strain without failing (Figure 2.1b). That means that it can take permanent deformation without losing its ability to support load. The test is usually stopped when the strain has reached a value of 5%. Rocks can be ductile or acquire a ductile behavior at high confining pressure and/or high temperature. This transition between brittle and ductile failure will be analyzed later in this chapter.

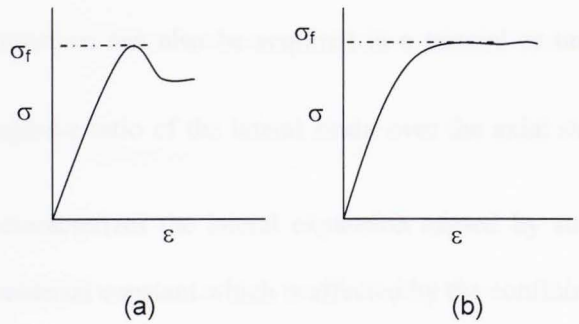


**Figure 2.1 Failure modes and stresses for (a) brittle and (b) ductile materials.**

### 2.1.2 Young's Modulus, E

One of the methods to characterize the material behavior is by analyzing the stress-axial strain plot. For most rocks and for stresses before failure, this plot

can be approximated by a straight line following Hooke's Law (Jaeger and Cook, 1979). This means that the strain of a sample is directly proportional to the stress. For uniaxial compression it can be represented by the equation $\mathbf{E}= \sigma \varepsilon_{\alpha}$ where **E** is Young's modulus, a material constant; $\sigma$ is the axial stress and $\varepsilon_{\alpha}$ is the strain measured in the axial direction. The theory of linear elasticity is based on the assumption that this equation holds accurately. The stress strain relation for rock can not be considered as linear; however, there is a portion of the stress strain plot that is linear. The calculation of Young's modulus is restricted to the linear portion of the stress-strain curve. Young's modulus is confining pressure dependent and increases as the confining pressure increases.

### 2.1.3 Poisson's ratio, ν

This information can also be acquired in a triaxial or uniaxial test. It is defined as the negative ratio of the lateral strain over the axial strain ($\nu = -\frac{\varepsilon_{L}}{\varepsilon_{a}}$). Poisson's ratio characterizes the lateral expansion caused by stress in the axial direction. It is a material constant which is affected by the confining pressure.

### 2.1.4 Dynamic moduli

The most common data provided to a petroleum engineer is usually velocities from logging tools. Due to the low relative cost compared to retrieving

a core, this is usually the only data available. The velocities of the shear and the compressional waves yield the dynamic Young's modulus, $E_D$, and the dynamic Poisson's ratio, $\nu_D$ (Birch, 1966). In the case of linear elastic materials, static and dynamic moduli should be the same. However, rock is neither isotropic nor linear. This can be proved by the hysterisis observed on the stress-strain plot when cycling the sample. Orientation, size and the shape of the cracks already present in the rock as well as created during the loading process affect the wave speed. In this study dynamic results are compared with static results obtained by multistage tests. For comparison purposes the static moduli have been calculated from the portion of the stress-strain plot where hydrostatic conditions are achieved ($\sigma_1 = \sigma_C$).

### 2.1.5 Mohr's plot, failure envelope, angle of friction and cohesive strength.

Otto Mohr was a German civil engineer who invented a convenient way to analyze the failure information of a rock on a single plot. The construction of this plot makes use of failure stresses ($\sigma_1$) obtained at different confining pressures ($\sigma_3$). The construction of the Mohr's plot starts by plotting the stresses $\sigma_1$ and $\sigma_3$. Then a semicircle is drawn with radius $\left(\frac{\sigma_1 - \sigma_3}{2}\right)$ starting from the point $\sigma_3$ and ending $\sigma_1$ on the x axis. This process is repeated until all the data available from triaxial tests at different confining pressures are plotted. The line tangent to those

circles is called the failure envelope and separates the plot into two different regions; the region of rock stability and instability, below and above the failure envelope line, respectively. The equation that describes this line is the Mohr-Coulomb failure criterion and is given by:

$\tau_n = \tan(\phi)\ \sigma_n + C$ .....(2.1)

where $\tau_n$ is the shear stress on the failure plane,

$\sigma_n$ is the normal stress on the failure plane,

$\phi$ is the angle of internal friction and,

C is the cohesion.

For any pair of axial and confining pressures located within the region of stability the rock will not fail (see Figure 2.2).

The ordinate and abscissa of a Mohr's plot are the shear or deviatoric stress $\left(\frac{\sigma_1 - \sigma_3}{2}\right)$ and the normal stress $\left(\frac{\sigma_1 + \sigma_3}{2}\right)$. At failure these are the magnitudes of shear and normal stress on the failure plane. The failure envelope intersects the y-axis at a point which is called the cohesive strength of the rock, C. This point can also be found by performing a simple shear test. It is the strength of the rock when the only stress applied is shear. The slope of this failure envelope gives the angle of the internal friction of the rock, $\phi$, which is also correlated with the angle of the failure plane, $\beta$, through the relation:

$\beta = \pi/4 + \phi/2$ ..... (2.2)

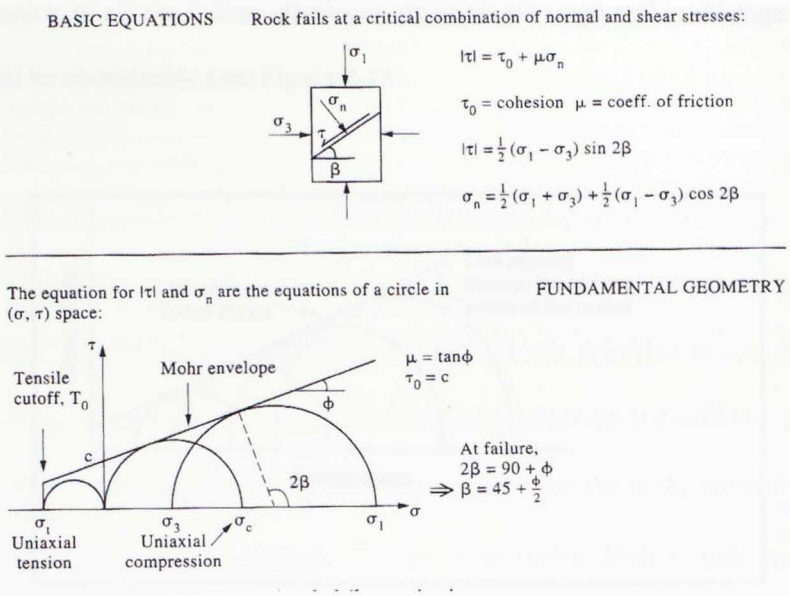


**Figure 2.2 Sketch of the Mohr's failure envelope and the Mohr's Coulomb failure criterion (Hudson and Harrison, 1997).**

This representation of rock strength is more comprehensive and provides additional insights than the single value of the unconfined strength of the rock UCS. The UCS is the maximum stress recorded before failure in a uniaxial experiment.

In this study for simplification, the line that is drawn is not the tangent to the circles (i.e. passing through the points $[0.5(\sigma_1-\sigma_3)\sin(2\beta), 0.5(\sigma_1+\sigma_3)+0.5(\sigma_1-\sigma_3)\cos(2\beta)]$) but is the line that passes from the highest point of the circle on the plot (i.e. passing through the points $[0.5(\sigma_1-\sigma_3), 0.5(\sigma_1+\sigma_3)]$). This will give a slightly different failure envelope. However if this technique is consistent for the

construction of all the failure envelopes using single stage and multistage results, they will be comparable (see Figure 2.3).

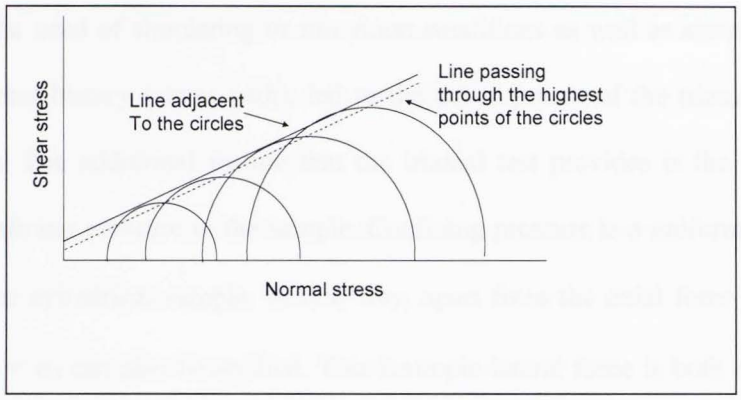


**Figure 2.3 Comparison of the two failure envelopes, first a line adjacent to the circles and second the simplified line that passes through the $\tau_{max}$.**

## *2.2 Evaluation of testing and capabilities*

### 2.2.1 Uniaxial test

A uniaxial test is a simple way to obtain mechanical properties. The apparatus simply applies axial load on a cylindrical plug. Two strain gages are mounted on the sample giving information about lateral and axial deformation. With this information, E, $\nu$ and $\sigma_f$ can be calculated. However this method has a major drawback. There is no way to apply either confining pressure, $\sigma_c$, or pore pressure, $\sigma_p$. Consequently, the uniaxial test can not simulate *in situ* stress conditions.

### 2.2.2 Triaxial test

The need of simulating *in situ* stress conditions as well as simulating the rock's stress history (stress path), led to the development of the triaxial testing apparatus. The additional feature that the triaxial test provides is the ability to apply confining pressure to the sample. Confining pressure is a uniform pressure around the cylindrical sample. In that way, apart from the axial force $\sigma_1$, other forces $\sigma_2 = \sigma_3$ can also be applied. This isotropic lateral force is both $\sigma_2$ and $\sigma_3$ and is usually called $\sigma_3$. However, even though it is a triaxial test, as there are forces applied from all three directions, only two of them can actually be adjusted independently. This is the reason why the name biaxial would be more suitable than triaxial. However, this is the conventional name for these tests so it is used in this study. The axial load is applied by a hydraulically driven piston, independent of the lateral loads. The first apparatus to perform this test was introduced in 1911 by Karman.

In the early times of testing, the only feedback for controlling the test was axial load increment. Currently, tests can be controlled by either load or deformation. Using very fast and sophisticated servo valves it is possible to control and maintain a constant axial strain rate. Using a computer, the strain is measured at very small time intervals and feedback signals are sent to the axial

control system, adjusting the axial load accordingly. This allows precise control over the test conditions and also allows post failure behavior to be observed. Pore pressure can also be controlled.

The sample is wrapped in a rubber or copper jacket, isolating it from the confining fluids in the vessel. Water or other fluids can be run through the sample creating pore pressure (Figure 2.4).

Temperature is another variable that can be controlled. Heat can be applied to the sample either by heating the copper jacket or heating the fluid that applies the confining pressure from outside the pressure vessel.

For this study, tests were conducted in a servo-controlled hydraulic press MTS-215. The maximum force that the hydraulic piston can apply is 350,000 pounds and the maximum confining or pore pressure it can apply is 20,000 psi.

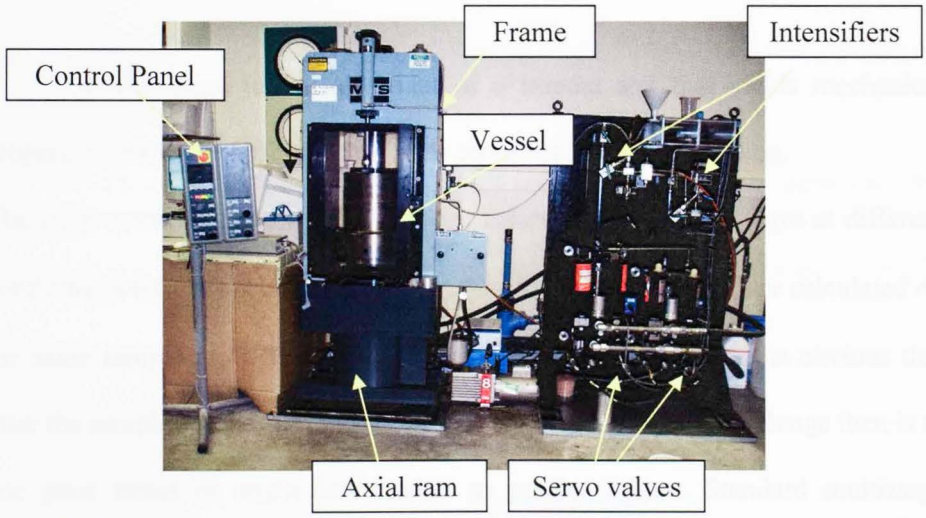


**Figure 2.4 Triaxial testing frame used for this study. On the left is the pressure vessel and on the right are the intensifiers for the pore and the confining pressure as well as the servo valves.**

### 2.2.3 Polyaxial test

In an effort to investigate the impact of the intermediate principal stress component, the polyaxial (or true triaxial) testing system was invented. This apparatus consists of three pistons that independently apply force from x, y and z directions. This test continues to have limitations. Such limitations would be the shape of the sample, which needs to be cubical as well as frictional issues between the platens and the sample. Furthermore, the stress is not applied uniformly. However, using this apparatus the effect of the intermediate stress on mechanical behavior has been studied (see Mogi, 1967).

### 2.2.4 Multistage technique

A multistage test is a variant of a triaxial test that yields mechanical properties of rock at different confining pressures from a single plug.

The *stage* portion of the word multistage refers to the loading stages at different confining pressures used during the test. The values of **E**, and $\nu$, are calculated on the same sample at different confining pressures. In this case, it is obvious that after the sample reaches failure, further testing is stopped. The challenge then is to use prior stress or strain information to predict failure. Standard multistage

methodologies, yield values for E, ν, ϕ and C which suggests the rocks are weaker than they actually are.

The proposed multistage technique attempts to recover mechanical properties which are equivalent to results obtained from conventional methods.

## 2.3 Volumetric strain as a monitoring parameter

The shape and the meaning of the volumetric strain will be extensively analyzed in this thesis because the success of the proposed multistage method strongly depends on it. The volumetric strain is used to provide an understanding of the failure process as well as the extent of the damage the rock has experienced at any stress stage. The volumetric strain provides distinctive, objective, easy to pick termination points which will make the testing repeatable and provide an index for the rock's condition.

Volumetric strain is defined as the fraction of change in volume over the initial volume ($\frac{\Delta V}{V}$). Assuming the sample is isotropic and the strains are small, the volumetric strain can be expressed as the summation of axial and lateral strains, and is given by:

$$\varepsilon_{vol} = \varepsilon_x + \varepsilon_y + \varepsilon_z \quad \text{.....(2.3)}$$

The fact that circumferential changes are measured instead of lateral changes in two different directions, guarantees that there will be no miscalculations due to localized variations in displacements. Assuming the rock is isotropic strains in the $\varepsilon_x$ and $\varepsilon_y$ directions are equal and are referred to simply as lateral strain $\varepsilon_L$.

The volumetric strain is calculated and plotted in real-time along with the measured axial and lateral strain. The shape of the volumetric strain yields more insight into changes taking place as the sample deforms. As such, it provides a reliable indicator of fracture initiation. Many studies have been conducted in relating the behavior of the volumetric strain with fracture initiation (see for example Brace et al., 1966).

Brace et al. (1966), divided the volumetric strain into four stages (see Figure2.5). The first stage is slightly concaved upwards. During this stage the cracks oriented perpendicular to the applied stress close. The extent of this stage depends on the number of cracks in the sample. Stage II is the linear elastic portion of the $\sigma-\varepsilon$ curve. It is possible to load and unload in this region without observing any hysterisis. In stage III grains may move and slide causing an inelastic behavior of the rock under pressure as well as propagate. New cracks are created in stage III too. The last stage, stage IV, is characterized by uncontrolled crack propagation, growth, creation and coalescing to form the final failure plane. This is the last stage before failure.

The main purpose of this study is to acquire the mechanical properties of the rock over stress regimes in which the failure process has not been initiated. Knowing when to stop applying stress on each loading cycle is therefore critical in controlling multistage tests. The characteristics of the volumetric strain as mentioned above are essential for this study.

During the first two stages, the rock deforms elastically. This can be proved by loading and unloading the sample at different stress levels and measuring the change of volume at the end of each loading cycle. Figure 2.6 shows that, if the amount of load does not exceed a value C' which defines the end of region II, there is no residual strain. Residual strain is defined as the amount of strain that is not recovered after removing the load. If the applied load exceeds the stress at C' then the volumetric strain does not fully recover. This effect can be also shown in the axial strain. However C', where the stage II ends is more obvious on the volumetric strain. It is the point where the volumetric strain deviates from a straight line.

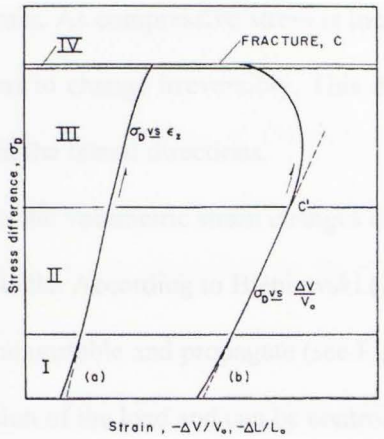


**Figure 2.5 Idealized (a) axial strain and (b) volumetric strain plotted against stress difference divided into four regions as described in text . Region I, crack closure; region II, linear part of deformation; region III, crack initiation; region IV, failure (Brace et al., 1966).**

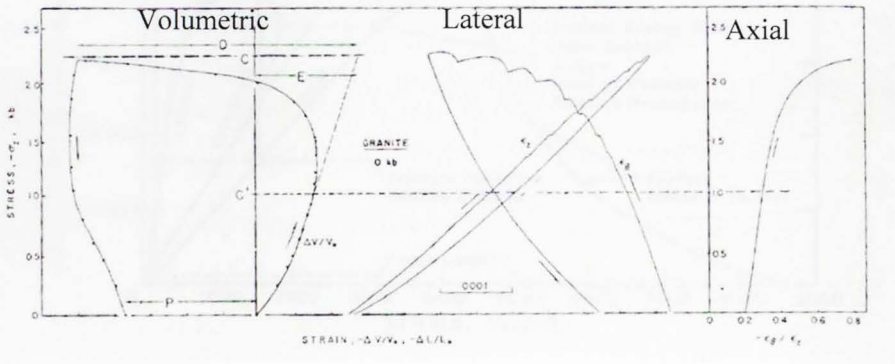


**Figure 2.6 Diagram of the volumetric strain, showing the C' point above which, cracks are being created on the sample. Before reaching the C' point there is no hysterisis in the axial and lateral strain during loading and unloading (Brace et al., 1966).**

The axial strain does not show a significant irreversible change and is not a very sensitive indicator of the processes leading to failure. However this is not

the case for the lateral strain. As compressive stress is increased beyond the point C' the lateral strain begins to change irreversibly. This means that beyond point C' cracks are expanding in the lateral directions.

Failure starts when the volumetric strain changes direction and crack propagation becomes unstable. According to Bieniawski (1967), above a critical stress level, cracks become unstable and propagate (see Figure 2.7). Prior to this, crack extension is a function of the load and can be controlled.

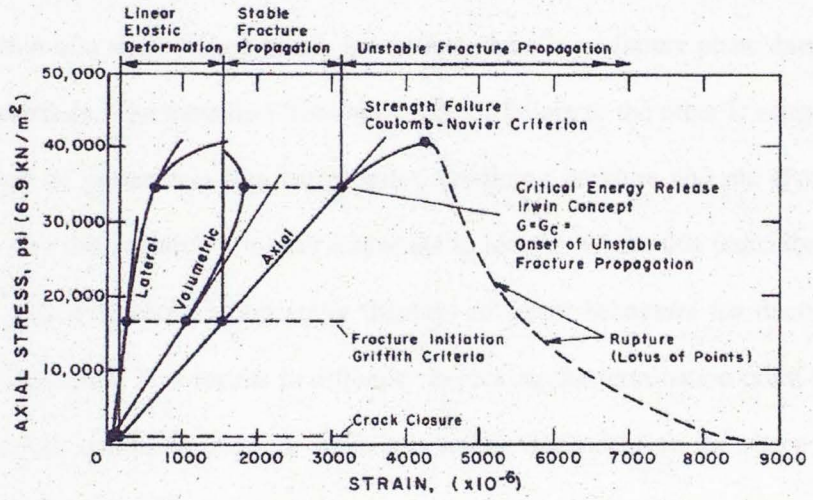


**Figure 2.7 Bieniawski's analysis of the volumetric strain (Bieniawski, 1967).**

## 2.4 Rheological considerations. Brittle-Ductile Transition

In experiments that require testing at different confining pressures, the rheological behavior of the rock has to be taken into consideration. The method that is proposed in this study is very dependent on the shape and the behavior of the volumetric strain curve. Tests showed that the volumetric strain curve has a repeatable shape for tests performed under conditions that allowed brittle failure.

Brittle failure is characterized by the concentration of microcracks and the formation of a shear failure plane. In contrast, there is no failure plane during the ductile failure. The transition from one mode of failure to the other is sensitive to a variety of parameters like temperature, confining pressure and etc (Paterson, 1978). For this research it is very important to identify where this transition takes place. The volumetric strain curve displays different behaviors for ductile and brittle materials. This results in difficulty in picking the termination point for the test at each confining pressure since it is totally dependent on the shape of the volumetric strain curve.

Performing tests at different confining pressures, yields information which is used to define the brittle ductile regimes for a rock. However, there are other methods to predict this transition. This is important for the multistage test because as will be explained later, mechanical data obtained at confining pressures that

promote ductile failure can not be used for the construction of the failure envelope.

The fact that the rock changes from brittle to ductile mode of failure has been shown as early as 1911 by Karman in studies on Carrara marble. Since then, other researchers (Handin and Hager, 1957; Paterson, 1978; Heard, 1960; Mogi, 1966 and Byerlee, 1968) have studied controls on the brittle-ductile transition. A large drop in the differential stress is typically observed during the brittle failure of rock. However, according to Orowan (1960), at high confining pressures the friction on the failure plane can be sufficient to prevent of this stress drop. The brittle-ductile transition will occur when the confining pressure is high enough to produce friction on the failure plane greater than the applied differential stress (Orowan, 1960).

Most brittle-ductile failure transition theories are based on friction theories. After testing a number of igneous rocks at high confining pressures, Mogi (1966) defined a line in differential versus confining pressure space that separates these behaviors. The line is reproduced in Figure 2.8. The linear function requires that the friction coefficient is independent of confining pressure. Byerlee (1968) later showed the coefficient of friction is dependent on confining pressure. Based on new experimental results, Byerlee (1978) showed that the angle of friction is not a constant but changes with the confining pressure. He found that the angle the failure plane makes with $\sigma_1$, $\theta$, for rocks (limestone,

serpentine, gabbro, dunite, granite) that failed near the brittle ductile transition zone was universally about 30 degrees. The equations describing failure which include the variation in angle of failure plane the normal and the shear stress on the failure plane are;

$$\tau = \frac{\Delta\sigma}{2}\sin 2\theta \quad \text{.....(2.4)}$$

$$\sigma_n = \frac{\Delta\sigma + 2\sigma_c}{2} - \frac{\Delta\sigma}{2}\cos 2\theta \quad \text{.....(2.5)}$$

where $\Delta\sigma$ = differential stress ($\sigma_1 - \sigma_3$)

$\sigma_c$ = confining pressure

Substituting the angle of the failure plane $\theta$ equal to 30 degrees and after transforming these two equations to the $\Delta\sigma$–$\sigma_c$ space, we obtain:

$$\Delta\sigma = 2.31\tau \quad \text{.....(2.6)}$$

$$\sigma_c = \sigma_n - 0.58\tau \quad \text{.....(2.7)}$$

According to Byerlee (1968) the rock will show ductile failure if at any given confining stress, the differential stress falls above the solid line on Figure 2.8. In this figure, both lines (Byerlee, 1968 and Mogi, 1966) have been plotted. For rocks failing at low differential stresses these two lines are very similar but Mogi's line describes the transition better. At higher confining pressures and for stronger rocks Byerlee's line seems to provide a better description. Above two kilobars (≈29,000 psi) of confining pressure this relation becomes linear. The

explanation for this phenomenon is that below two kilobars sliding in the failure plane happens by raising over the irregularities of the surface. However, above the confining pressure of two kilobars it is easier to shear these irregularities. Bernabe and Brace (1990) tested Berea sandstone at different confining and pore pressures, and concluded that the brittle to ductile transition, takes place at 40 MPa confining pressure (Figure 2.9).

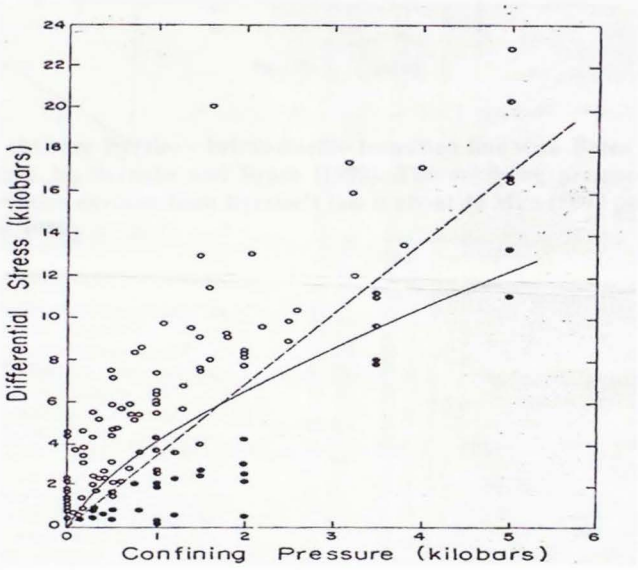


**Figure 2.8 Observations of failure modes for mainly igneous and metamorphic rocks (Mogi, 1966 and Byerlee, 1968). The open circles represent brittle failure, whereas the closed circles represent ductile failure. The dotted line is Mogi's transition between brittle and ductile failure and the solid line is Byerlee's transition. Note that at low stresses the transition is better described by Mogi's approach (Byerlee, 1968).**

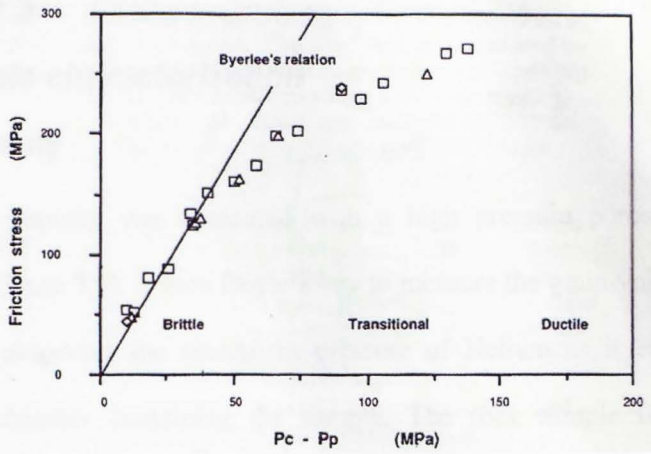


**Figure 2.9 Plot showing Byerlee's brittle-ductile transition line with Berea sandstone data obtained by Bernabe and Brace (1990). The confining pressure at which the observation deviates from Byerlee's line is about 40 MPa (5800 psi) (Bernabe and Brace, 1990).**

# Chapter 3

## *3.1 Sample characterization*

### 3.1.1 Porosity

The porosity was measured with a high pressure porosimeter (HPP) apparatus (Figure 3.1). It uses Boyle's law to measure the grain volume of a core sample by observing the change in pressure of Helium as it expands into a calibrated chamber containing the sample. The rock sample is placed in a chamber of known volume. Helium is held in a reference chamber of known volume and pressure, typically 100 psi. The two chambers are connected, causing the helium to drop in pressure as it fills the sample chamber and the pores in the sample. The only volume not filled is the grain volume and the isolated pores. Neglecting the latter, the grain volume can then be calculated from Boyle's Law using the pressure before and after connecting the chambers. The apparatus is calibrated against a quartz crystal of known grain volume.

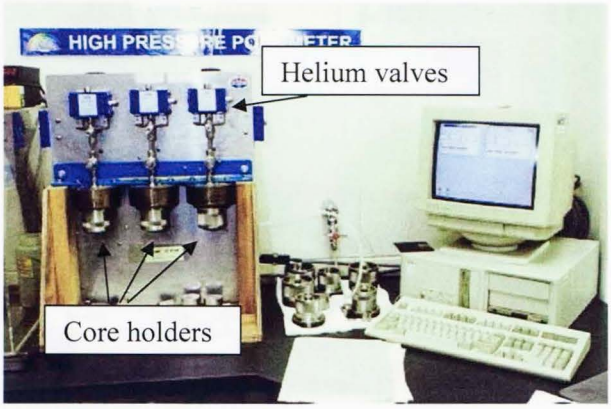


**Figure 3.1 Automated porosimeter apparatus in the IC[3] laboratory.**

### 3.1.2 Permeability

Permeability is defined as an intrinsic rock property. In practice the actual value one measures depends upon both the technique and the fluids used for the measurement. For example, apparent permeability measured with gas has to be corrected to yield equivalent liquid permeability, the well known Klinkenberg corrected permeability. To calculate the permeability of a rock the gas permeability at three or more different pressure points are plotted against the inverse of pressure (1/P) and then the graph is extrapolated to infinite pressures.

In this study, the CMS-300* apparatus was used for the measurements of permeability (Figure 3.2). It calculates permeability from non-steady state pressure measurements (Stanley 1972). The apparatus has the ability to measure permeability and porosity at different confining pressures up to 10,000 psi.

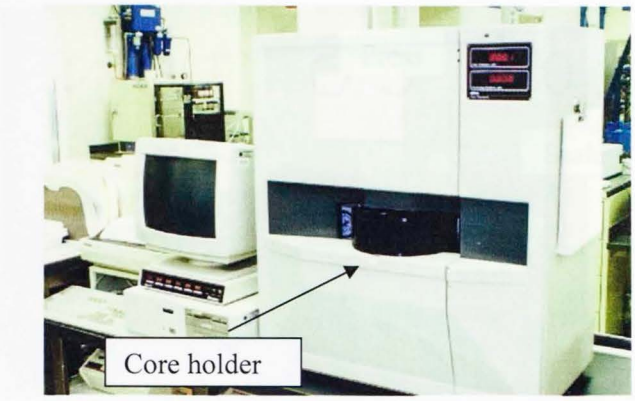


**Figure 3.2 CMS apparatus in the IC$^3$ laboratory.**

### 3.1.3 Mineralogy

The mineralogy is found from interpretation of infrared spectra. The fact that the mineral structures have characteristic and reproducible absorptions spectra can be used and compared with known standards. A representative portion of a plug is pulverized, mixed with KBr and transformed into a transparent compacted disc resembling glass with the help of pressure. The sample is placed in the path of an infrared beam in the vacuum chamber of an FTIR (Fourier Transform Infra Red) apparatus (Figure 3.3). Using Fourier analysis the recorded spectrum can reveal the mineralogical composition of the plug.




**Figure 3.3 FTIR apparatus in the IC$^3$ laboratory. The scale is used to precisely weight the finely ground rock ssample and KBr. The press is used to form the mixture (KBr+sample) into a transparent pellet for testing.**

### 3.1.4 Photographs of failed samples

Digital photographs of the failed samples are presented in Appendix IV. These photographs show the orientation of the plane of failure, if it is visible. In Figure AIV.3 the pressure cone is visible. Due to friction between the steel endcaps and the sample at the area of contact, the sample is not free to expand laterally. The frictional constrains result in the formation of two cones that are less deformed than the rest of the rock. The area between the tips of these cones represents the part of the sample that is freely deformed.

### 3.1.5 Velocities

Finally the velocities of the compressional and the shear waves were recorded as a function of confining pressure. A pair of transducers was mounted on companion plugs of one inch diameter and two inch length. Velocities and densities were used to calculate the dynamic moduli.

## *3.2 Characterization summary*

Characterization of the plugs was carried out to assess the homogeneity of the samples chosen for this test. Homogeneity is expected, when dealing with samples from the same block having no visible differences (change of layering, color etc.). Thus, the plugs should display minimal variations in physical and chemical properties. The analysis that follows supports these expectations. The characterization tests performed before the mechanical tests, were FTIR, HPP, CMS and velocities. These tests are non-destructive and do not alter the mechanical properties of the rock.

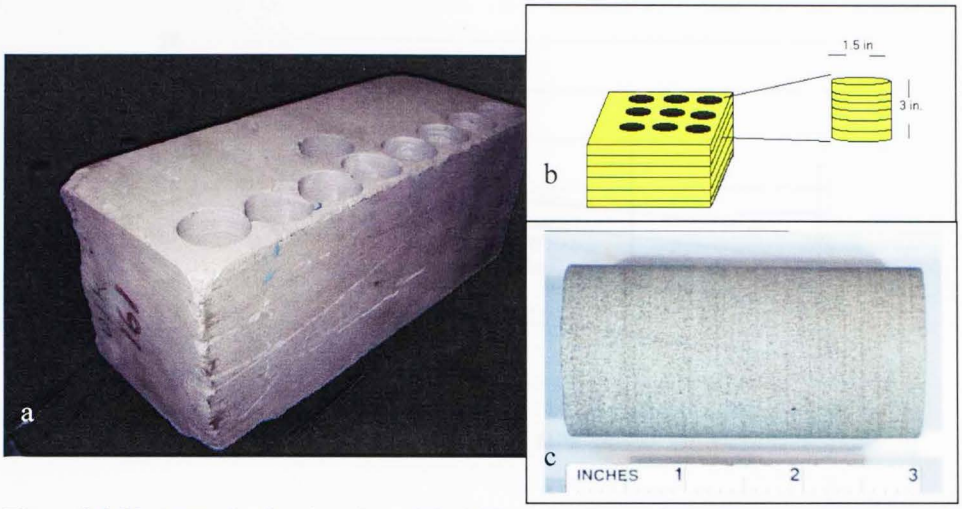


**Figure 3.4 Photograph, showing the original block (a) from which samples (c) were cored. Inset b shows the orientation of the plugs relative to the bedding. Bedding planes are visible in plug sample shown (c).**

### 3.2.1 Porosity

The porosity of the samples was measured at five different confining pressures (3.45, 6.9, 17.21, 24.14, 34.18 MPa) using the CMS. The samples were cored from the same block of Berea so it is expected that the measured porosities be similar if not identical. Small differences in porosity reflect differences of the pore structure even for samples that are spatially close to each other. The results of the porosity measurements are presented in the graph shown in Figure 3.5.

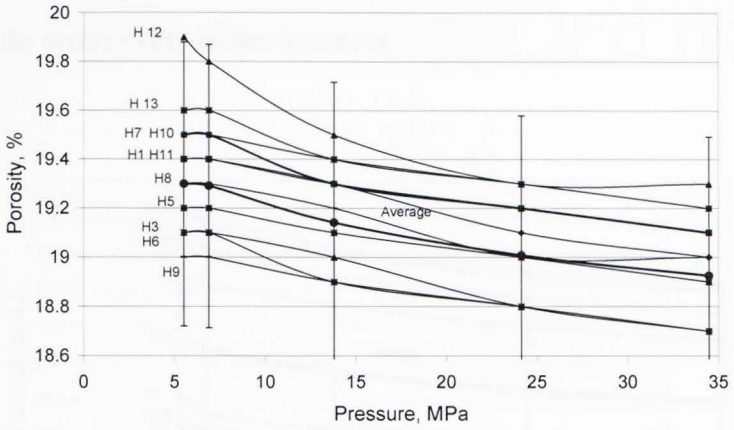


**Figure 3.5 Porosity as a function of confining pressure. Note that the maximum deviation from the average porosity is less than half a porosity unit. Porosities change less than 3% over the range of pressure.**

The difference in the porosities at a specific pressure is less than a porosity unit proving two points: first variations do exist, so the samples are not totally homogeneous; and second the differences are small. The equation that describes the variation of the average porosity with respect to confining pressure, $\sigma_c$, is:

$$\phi = -0.2119*\ln(\sigma_c) + 19.684 \quad \text{.....(3.1)}$$

where, the confining pressure is in MPa and porosity in %.

### 3.2.2 Permeability

The results of the permeability follow the same trend as porosity. Again we observe a slight variation in measured permeabilities among the samples

tested. We consider the 13% variation to be acceptable and for our purposes consider the permeability as homogeneous.

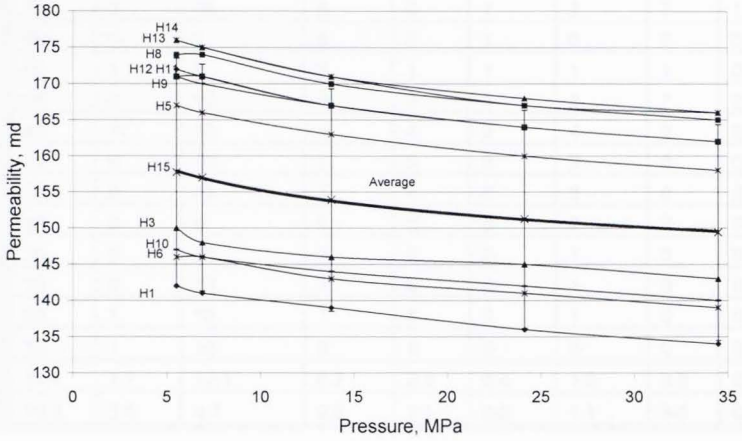


**Figure 3.6 Klinkenberg correct permeabilities as a function of confining pressure. The variability of permeability is only 13%. There is slight non-linear pressure dependence.**

Again the deviation is not very large. For the same confining pressure it is less than 40 millidarcies. In this case the equation that describes the variation of the permeability with respect to confining pressure, $\sigma_c$, is:

$$k = -4.565*\ln(\sigma_c) + 188.44 \quad \text{.....(3.2)}$$

where, the confining pressure is in MPa, and k is in md. The mineralogical analysis supports the homogeneity of the samples.

**Table 3.1 Mineralogical composition of 15 Berea sandstone samples. All values in weight %.**

| Sample # | Quartz | Calcite | Total Clays | Feldsp. | Pyrite | Anhyd. | Siderite | Dolo. | Chlor. |
|---|---|---|---|---|---|---|---|---|---|
| | % | % | % | % | % | % | % | % | % |
| H1 | 88 | 0 | 7 | 6 | 0 | 0 | 0 | 0 | 0 |
| H2 | 75 | 0 | 13 | 6 | 4 | 0 | 1 | 1 | 0 |
| H3 | 86 | 2 | 5 | 7 | 0 | 0 | 0 | 1 | 0 |
| H4 | 72 | 3 | 10 | 5 | 0 | 1 | 2 | 7 | 1 |
| H5 | 83 | 0 | 7 | 6 | 0 | 1 | 0 | 2 | 0 |
| H6 | 80 | 1 | 9 | 6 | 1 | 1 | 1 | 1 | 0 |
| H7 | 70 | 4 | 10 | 6 | 0 | 1 | 2 | 7 | 2 |
| H8 | 45 | 11 | 19 | 4 | 4 | 2 | 4 | 9 | 2 |
| H9 | 74 | 0 | 15 | 7 | 3 | 0 | 2 | 0 | 0 |
| H10 | 70 | 2 | 17 | 7 | 4 | 0 | 0 | 0 | 0 |
| H11 | 83 | 0 | 8 | 6 | 0 | 0 | 0 | 2 | 0 |
| H12 | 76 | 0 | 12 | 7 | 3 | 0 | 1 | 0 | 0 |
| H13 | 70 | 0 | 18 | 7 | 5 | 0 | 1 | 0 | 0 |
| H14 | 68 | 1 | 19 | 7 | 5 | 0 | 1 | 0 | 0 |
| H15 | 72 | 1 | 15 | 6 | 4 | 0 | 0 | 0 | 0 |
| Average | 74.1 | 1.7 | 12.3 | 6.2 | 2.2 | 0.4 | 1.0 | 2.0 | 0.3 |
| STDVEV | 10.3 | 2.9 | 4.7 | 0.9 | 2.1 | 0.6 | 1.1 | 3.0 | 0.7 |

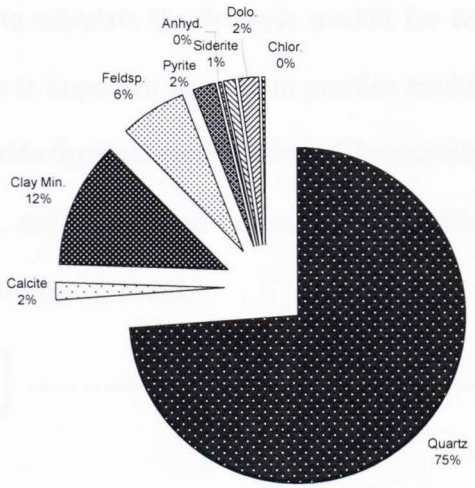


**Figure 3.7 Average mineral composition (weight percentage) for 15 samples of Berea sandstone used in this study. Mineralogy was determined by transmission FTIR . Note clay fraction is less than 12% and quartz dominates.**

Note that even though the plugs come from the same block there are still samples (plug H8) in which the mineralogical differences are quite large. However the rest of the samples were very similar in composition. The dominant mineral is quartz, accounting 75% of the matrix whereas the remainder is clay and feldspars. These three minerals combine to form 93% of the matrix.

### 3.2.3 Velocities

The velocities of the P- and S- waves were measured as a function of the confining pressure. The different confining pressures used for this test were similar to those used in the series of the mechanical tests. We used the velocities and the densities to calculate the dynamic moduli for comparison to measured static moduli. This is important because in practice moduli are derived from log data which also yields dynamic moduli values. The equations used to calculate the bulk modulus, $K_D$, and the Poisson's ratio, $\nu_D$, from velocities of compressional and shear waves are (Birch, 1966):

$$K_D = \rho\left(v_p^2 - \frac{3}{4}v_s^2\right) \quad \text{.....(3.3)}$$

$$\nu_D = \frac{\left(\frac{v_p}{v_s}\right)^2 - 2}{2\left(\left(\frac{v_p}{v_s}\right)^2 - 1\right)} \quad \text{.....(3.4)}$$

**Table 3.2 Compressional (P) and shear ($S_1$-$S_2$) wave velocities reported as a function of confining pressures. $S_1$ and $S_2$ are both shear wave velocities measured in the same direction but having orthogonal polarization.**

| | | Confining Pressure, psi | | | | | |
|---|---|---|---|---|---|---|---|
| | | 500 | 1000 | 1500 | 2500 | 3500 | 5000 |
| Sample # | Wave | (ft/sec) | (ft/sec) | (ft/sec) | (ft/sec) | (ft/sec) | (ft/sec) |
| H1 | P | 9954 | 11184 | 11821 | 12231 | 12535 | 12949 |
| | s1 | 5443 | 5998 | 6321 | 6711 | 7175 | 7393 |
| | s2 | 7012 | 7854 | 8259 | 8860 | 9280 | 9877 |
| H2 | P | 10165 | 11213 | 11803 | 12309 | 12679 | 12973 |
| | s1 | 6293 | 6936 | 7430 | 7860 | 8065 | 8281 |
| | s2 | 6202 | 6854 | 7270 | 7691 | 7894 | 8072 |
| H3 | P | 9373 | 10711 | 11462 | 12206 | 12679 | 13053 |
| | s1 | 5704 | 6361 | 6741 | 7157 | 7330 | 7485 |
| | s2 | 6745 | 7476 | 7929 | 8528 | 8895 | 9123 |
| H4 | P | 9070 | 10367 | 11178 | 11954 | 12479 | 12828 |
| | s1 | 5737 | 6410 | 6745 | 7280 | 7486 | 7684 |
| | s2 | 6562 | 7556 | 8307 | 8892 | 9164 | 9330 |
| H5 | P | 9142 | 10583 | 11442 | 12195 | 12616 | 12985 |
| | s1 | 6057 | 6879 | 7380 | 7854 | 8128 | 8353 |
| | s2 | 5947 | 6778 | 7291 | 7792 | 8019 | 8190 |
| H6 | P | 9041 | 10587 | 11384 | 12240 | 12679 | 12911 |
| | s1 | - | 6267 | 6678 | 7185 | 7554 | 7753 |
| | s2 | 6182 | 6927 | 7432 | 8217 | 8590 | 8938 |
| H7 | P | 9937 | 11353 | 12195 | 12648 | 12807 | 13137 |
| | s1 | 5838 | 6426 | 6858 | 7185 | 7460 | 7585 |
| | s2 | 6875 | 7915 | 8439 | 8860 | 9037 | 9284 |
| H8 | P | 9281 | 10721 | 11479 | 12263 | 12596 | 12963 |
| | s1 | 6031 | 6810 | 7359 | 7844 | 8105 | 8289 |
| | s2 | 6062 | 6768 | 7248 | 7719 | 7910 | 8136 |
| H9 | P | 9148 | 10535 | 11323 | 12166 | 12626 | 12904 |
| | s1 | 6111 | 6917 | 7396 | 7945 | 8212 | 8424 |
| | s2 | 6014 | 6864 | 7419 | 7929 | 8149 | 8299 |
| H10 | P | 9191 | 10660 | 11325 | 12134 | 12569 | 12971 |
| | s1 | 6061 | 6805 | 7335 | 7849 | 8091 | 8308 |
| | s2 | 5988 | 6747 | 7219 | 7773 | 7997 | 8184 |
| H11 | P | 9391 | 10878 | 11571 | 12210 | 12761 | 13226 |
| | s1 | 5787 | 6555 | 6997 | 7309 | 7503 | 7638 |
| | s2 | 6851 | 7869 | 8529 | 9045 | 9344 | 9682 |
| H12 | P | 8974 | 10465 | 11320 | 12139 | 12495 | 12872 |
| | s1 | 6018 | 6843 | 7323 | 7863 | 8152 | 8349 |
| | s2 | 6002 | 6814 | 7308 | 7868 | 8098 | 8305 |
| H13 | P | 9620 | 10901 | 11776 | 12226 | 12575 | 12993 |
| | s1 | 5634 | 6199 | 6594 | 6987 | 7172 | 7306 |
| | s2 | 6526 | 7389 | 7921 | 8535 | 8857 | 9157 |

### 3.2.4 Sample preparation

The preparation of the specimen is described in ASTM (D2664-80). The length over diameter ratio has to be greater than two to avoid the pressure cone phenomenon. It describes a non-uniform distribution of the lateral displacement along the sides of the specimen. Friction develops between the sample and the platens at the area of contact preventing the sample from expanding in the lateral direction. Figure 3.8 (Hawkes and Mellor, 1970) shows the calculated stress intensity contours along the sample plug. The maximum stress was found to appear in the grey zones shown in Figure 3.8. Solution for this problem, in case there is insufficient length of core, is lubrication of those surfaces or the use of spacers made of the same material. There are also empirical equations (Weidinger et al., 1996) to correct for various specimen lengths but it is always advisable the use of sufficiently long core.

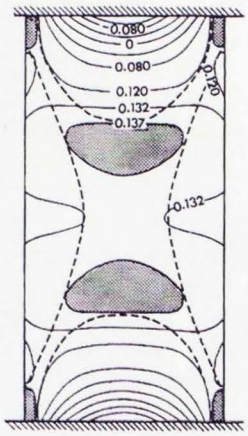


**Figure 3.8 Stress distribution for a uniaxial test. Contours represent relative intensity of maximum stress (Hawkes and Mellor, 1970).**

One and a half inch (3.81 cm) diameter samples were cored vertically with respect to the bedding. A length to diameter ratio of 2:1 was maintained. The two ends were polished flat and parallel departing no more than 0.0005 in. (0.0127 mm) from plane surfaces, in accordance to the ASTM guidelines (D2664-80) for triaxial testing. The samples were cleaned in a Soxhlet extractor and dried in a vacuum oven at 100 $^{o}$C.

Samples were removed from the oven and allowed to cool in a dessicator for two hours before being tested. Tests were performed under dry conditions. Samples were jacketed in polyolefin heat shrink tubing and sealed to the endcaps with twisted copper wire.



**Figure 3.9 Preparation of the sample. Heating the polyolefin tube on the sample to provide an impermeable barrier to confining pressure.**

After applying the heat-shrink tubing, the chain of the cord travel gage is wrapped around the sample and the two pins of the gage are set firmly against the jacket. We measure lateral expansion with a circumferential gage (Figure 3.10). This gage measures the change in circumference directly and not the lateral expansion. It produces an 'average' lateral strain value that is insensitive to local or directional variations in lateral strain. The equations below are used to transform the gage output to circumference change ΔC and eventually lateral strain.

$$\Delta C = \frac{\Delta l \pi}{\sin\left(\frac{\theta_i}{2}\right) + \left(\pi - \frac{\theta_i}{2}\right)\cos\left(\frac{\theta_1}{2}\right)} \quad \text{.....(3.5)}$$

where $\theta_i$ is defined as:

$$\theta_i = 2\pi - \frac{l_c}{(R_i + r)} \quad \text{.....(3.6)}$$

$\Delta l$ is the extensometer output,

$l_c$ is the length of the chain,

$R_i$ is the initial radius of the specimen,

$r$ is the radius of the roller of the chain.

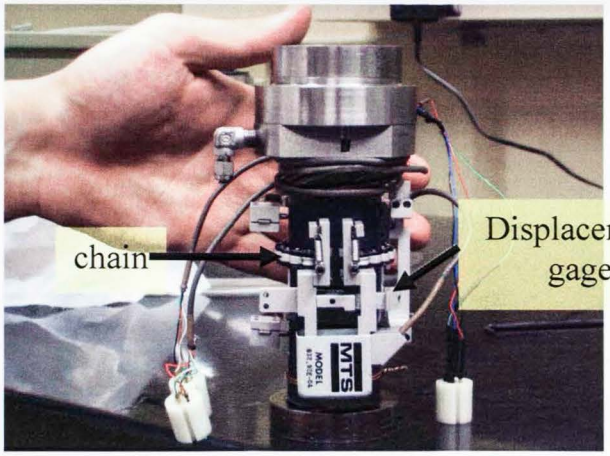


**Figure 3.10 The lateral extensometer mounted on the sample.**

Another gage measures the axial displacement over a gage length of two inches. Extra caution has to be used to make sure that the two pins are aligned in the vertical direction (Figure 3.11) and they are firmly set against the jacketed material.

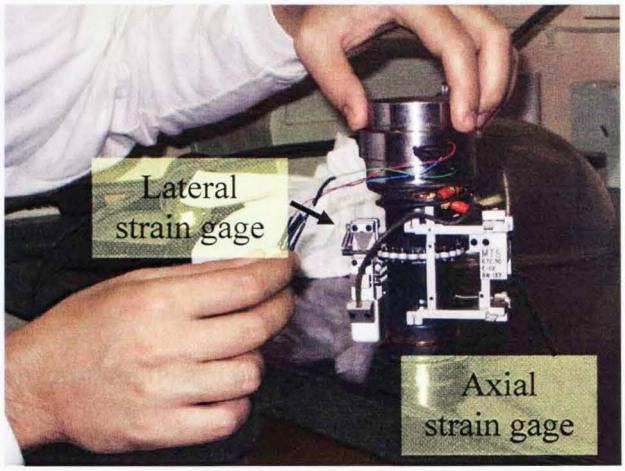


**Figure 3.11 Both lateral and axial extensometers mounted on the sample.**

# Chapter 4

## *4.1 Multistage methods; a review*

### 4.1.1 Literature review

Obtaining the failure envelope from a single plug should have wide applications in industry. A number of scientists have suggested different approaches to perform multistage tests. A goal of this study is to design a test that will yield a failure envelope from a single plug comparable to one obtained using the conventional technique. The research is focused on two fundamental issues; first where should the test be stopped for each loading stage and confining pressure; and second what loading path should be followed. One approach dictates that the test should be stopped when the sample shows signs of failure. A second approach makes use of the $\varepsilon_{vol}$ and stops the test when $\varepsilon_{vol} = 0$ (Crawford and Wylie, 1987). Most researchers (Kim and Ko, 1979; Kovari et al., 1983 and Harouaka et al., 1995) focused on the first approach. The second method (Crawford and Wylie, 1987) was proposed for use when dealing with very soft loading frames.

### 4.1.2 The "sign of failure" criterion

One of the early works on the multistage technique was done by Kim and Ko, (1979). They used a multistage technique to test three different types of rock; Pierre shale, Raton shale and Lyons sandstone. The stress path they used involved

applying an initial confining pressure followed by loading the sample until it showed signs of failure. At that point the test was halted and the confining pressure was increased to the next level without removing the axial load. This procedure was repeated for as many confining pressures as required. 'Sign of failure' was defined as the plateau of the stress-axial strain plot after leaving the elastic region.

Kovari et al. (1975), cycled the same sample under constant confining pressure for a number of test loadings to peak stress. They reported that the differences of these peak stresses obtained from these cycles were small and were considered negligible. Their studies were conducted on Buchberg sandstone and Carrara marble. They concluded that rock can go through a number of strength peaks with negligible variation of the peak strength stress.

The error Kim and Ko (1979), observed in the failure envelope characteristics (C, $\phi$) for the Lyons sandstone was 19% for the angle of friction, $\phi$, and 38% for the cohesion, C, (see Figure 4.1). Both errors are quite large. The errors are substantially less in the case of shale where the error in $\phi$ is $\pm$19% and the error in C term is $\pm$12% (see Table 4.1).

An explanation for this large difference in errors may be found in the rheology differences between these lithologies. Shale exhibits ductile behavior, failure prediction can be made without risking the integrity of the sample. Tests can be run near peak stress without the fear of failure. While shale shows signs of

failure within a narrow range of stress, the strain interval is relatively large. However, in brittle failure the axial stain curve starts diverting from a straight line at about 80% of the failure stress, and failure occurs almost instantaneously. Thus, deciding where to stop the test becomes subjective and very risky for brittle materials. Kim and Ko (1979) thus state that the effectiveness of the multistage test depends on the type of failure that the rock is expected to have. This makes this method inapplicable for brittle rocks at low confining pressures.

**Table 4.1 Summary Kim and Ko's results, comparing multistage and single stage tests (data obtained from Kim and Ko, 1975). Note the large error in the case of the brittle sandstone, in contrast to the ductile shale.**

| Rock Type | Test Type | Friction angle (degrees) | Cohesion (MPa) |
|---|---|---|---|
| Pierre shale | | | |
| | Multistage | 4 | 1.41 |
| | Single Stage | 6 | 1.42 |
| | Error | 23% | 1% |
| Raton Shale | | | |
| | Multistage | 29 | 41 |
| | Single Stage | 23 | 46 |
| | Error | 19% | 12% |
| Lyons Sandstone | | | |
| | Multistage | 48 | 45 |
| | Single Stage | 59 | 28 |
| | Error | 19% | 38% |

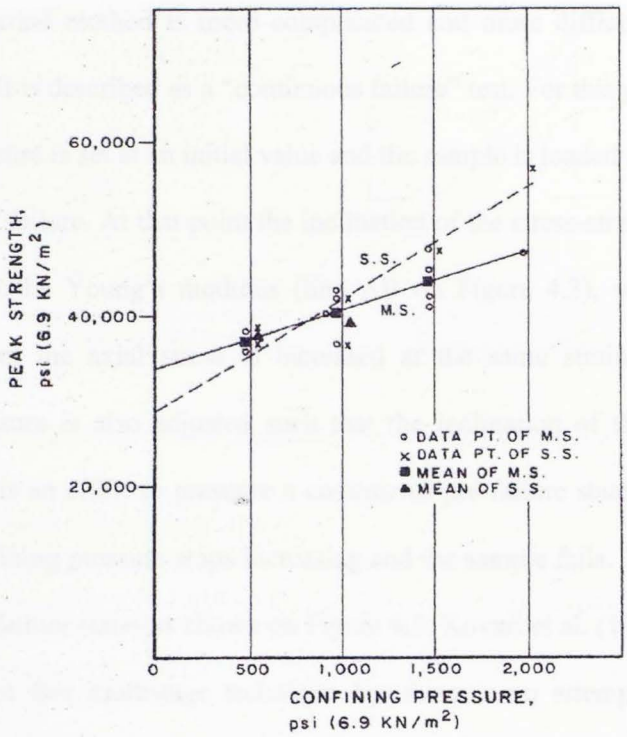


**Figure 4.1 Results of multistage (M.S.) and single stage (S.S.) triaxial tests for Lyons sandstone by Kim and Ko (1979).**

Kovari et al. (1983) used two different techniques in performing multistage tests. The first one is almost the same as the approach used by Kim and Ko (1979) (Figure 4.2b). The same stress path was followed and tests were terminated at the peak strength at each confining pressure. They define peak strength as the maximum axial stress which the intact specimen can support at a given confining pressure. However, they do not report a comparison of the failure envelopes obtained from conventional testing and their method.

The second method is more complicated and more difficult to perform (Figure 4.2c). It is described as a "continuous failure" test. For this procedure, the confining pressure is set at an initial value and the sample is loaded axially until it shows signs of failure. At that point the inclination of the stress-strain plot, which corresponds to the Young's modulus (line AB on Figure 4.3), was measured. After that point the axial stress is increased at the same strain rate but the confining pressure is also adjusted such that the inclination of the AB line is maintained. It is an effort to preserve a continuous pre-failure state until the end where the confining pressure stops increasing and the sample fails. This test gives a sequence of failure states as shown on Figure 4.3. Kovari et al. (1983) detail the methodology of this multistage technique but there is no attempt to compare results of this method with those from conventional tests.

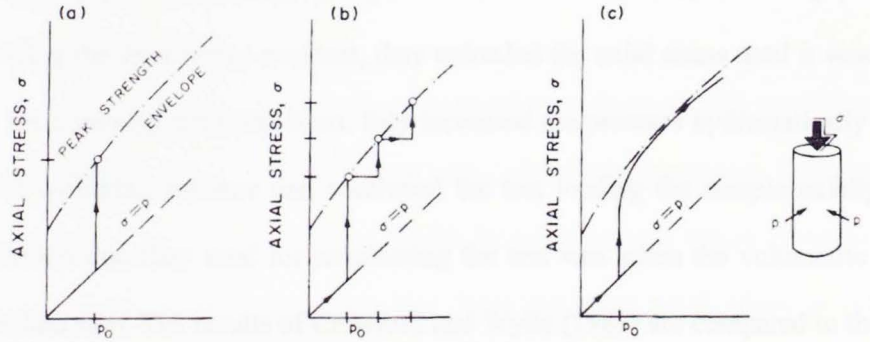


Different triaxial test types: (a) Type I—individual test; (b) Type II—multiple failure state test; (c) Type III—continuous failure state test.

**Figure 4.2 Stress paths followed in tests by Kovari et al. (1983).**

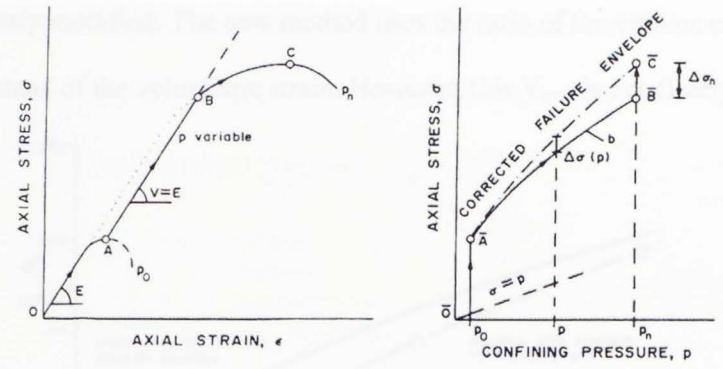


**Figure 4.3 Construction of the failure envelope using the method proposed by Kovari et al. (1983).**

### 4.1.3 Using the volumetric strain

Crawford and Wylie (1987) were the first to use the volumetric strain as a criterion to determine the termination point of each cycle. They used a different loading path from the studies mentioned above. Instead of increasing the confining pressure after stopping the test to meet the next confining pressure, holding the axial stress constant, they unloaded the axial stress until it was equal to the confining pressure. Next, they increased the pressure hydrostatically to the next confining pressure and continued the test loading the sample axially. The criterion that they used for terminating the test was when the volumetric strain reached zero. The results of Crawford and Wylie (1987) are compared to the ones obtained by the conventional method (see Figure 4.4). The authors mention that there were tests where failure occurred prior to the end of the planned multistage test. Typically, this was used for brittle materials and the method was

subsequently modified. The new method uses the ratio of the volume change over a $V_{max}$ instead of the volumetric strain. However, this $V_{max}$ is not clearly defined.

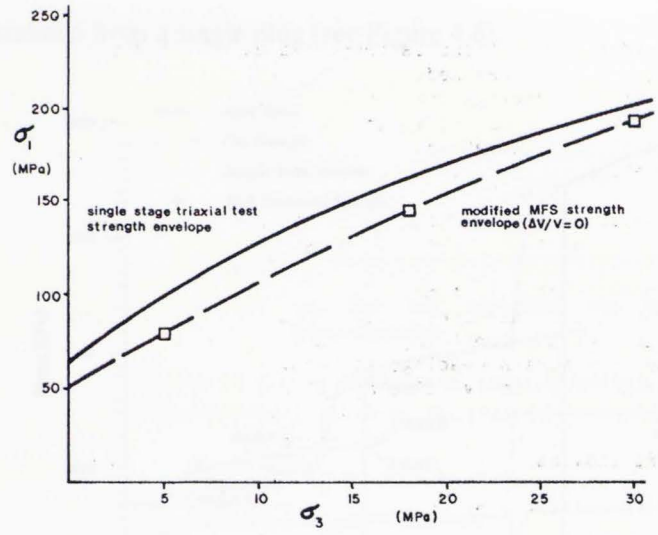


**Figure 4.4 Comparison between multistage and single stage triaxial test results by Crawford and Wylie (1987). Note that this envelope is lower than that obtained from the conventional tests.**

At this point, for the sake of completeness Bro's (1995) work should be mentioned. He performed multistage tests using strain hardening. Following the same loading path as Kim and Ko (1979), he calculated the failure envelope using points on the stress-strain curve that have the same axial strain at different confining pressures; this is physically impossible. He had to extrapolate the stress-strain plot of a stage with greater values of axial strain. For a better understanding, the stress-strain plot is given in Figure 4.5. Section C is extrapolated giving the

point G. Points G and F both have the same axial strain for different confining pressures during one single test. His conclusion is a strain dependent C and $\phi$ that can by calculated from a single plug (see Figure 4.6).

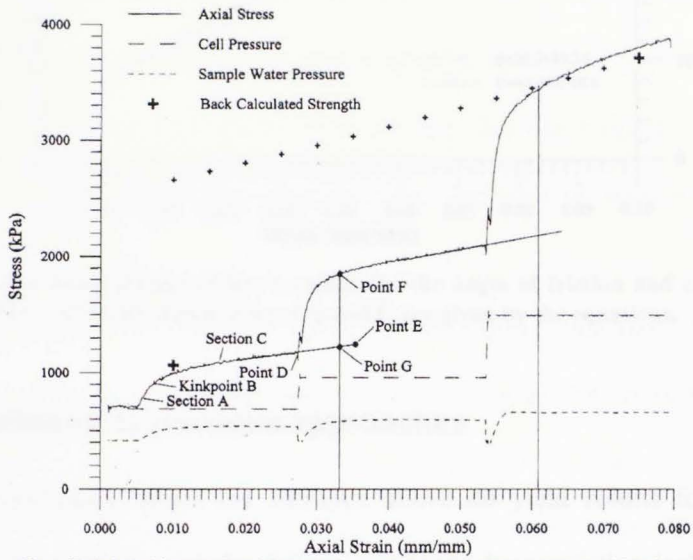

Fig. 1. Typical triaxial test result—axial stress, cell pressure and sample water pressure vs axial strain.

**Figure 4.5 Multistage testing used by Bro (1995). Points F and G have the same axial strain at different confining pressures. Point G is fictitious as it created by extrapolating section C (Bro, 1995).**

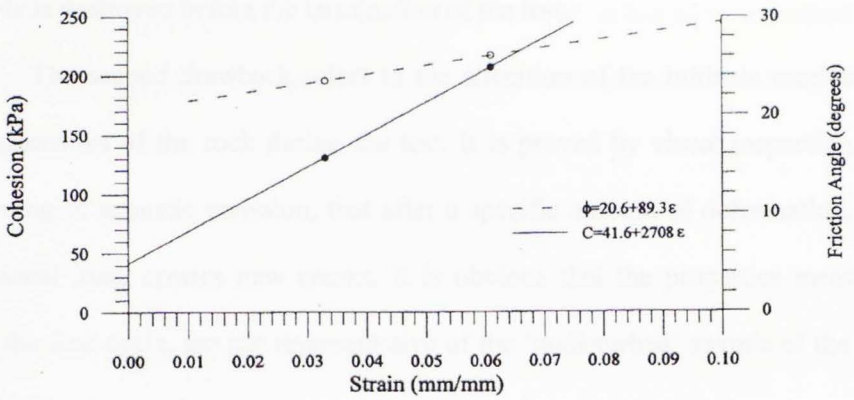


**Figure 4.6 Strain dependencies of Bro's results for the angle of friction and cohesion Bro (1995). The strain dependency of ϕ and C are given by the equations.**

### 4.1.4 Drawbacks to previous approaches

As mentioned before the methods above do yield results for ultimate strength, elastic moduli, and the failure envelope characteristics (cohesion and angle of friction) of rock. However, there are three substantial drawbacks to these multistage testing methods. The first major drawback is that the sample is put to great risk. In both cases, either when using $\varepsilon_{vol} = 0$ to stop the test on each loading cycle (Crawford and Wylie, 1987) or when using the axial strain deflection, as the sign of failure; (Kim and Ko, 1979; Kovari et al., 1983 and Harouaka et al., 1995). Premature failure can occur. Failure cannot be controlled for all cases, especially when the rock is stressed beyond the region of the stable crack propagation. Depending on the material and the confining pressure applied on the

sample, the failure can be sudden, without any precursory signs. In that case, the sample is destroyed before the termination of the test.

The second drawback refers to the alteration of the intrinsic mechanical characteristics of the rock during the test. It is proved by visual inspection and recording of acoustic emission, that after a specific amount of deformation, any additional load, creates new cracks. It is obvious that the properties measured after the first cycle, are not representative of the 'undisturbed' sample of the first confining pressure stage.

Subjectivity is the third drawback of the existing multistage techniques. Observing the results of previous research, it is obvious that even though the difference in the peak strength between the multistage and the single stage is small, the failure envelope produced has a considerable error. This can be explained by the fact that the operator cannot confidently recognize the peak strength and terminates the test prematurely. This results in a failure envelope which suggests the rock is weaker than it actually is.

The method that is proposed in this study attempts to account for the three shortcomings of the current methods. The new method has to guarantee that the sample will remain intact until the completion of the test. That is, until we get all the information we need from this sample. Furthermore, the mechanical properties obtained at each confining pressure stage have to be representative of the original intact sample without fatiguing the sample. Last but not least and probably most

important is that this method has to yield results that are comparable to the values obtained by the conventional multiple sample method. It has to be a method that minimizes errors due to operator subjectivity and should be an easy and repeatable procedure.

# Chapter 5

## 5.1 The proposed method

### 5.1.1 Introduction

A multistage test refers to a triaxial testing method where a single rock plug is tested under different confining pressures until it finally fails. The objective is to define a complete failure envelope which will provide the cohesive strength, C, and angle of friction, $\phi$, as well as the values of E, $\nu$, at various confining pressures.

In this study, plugs from a common block of Berea sandstone were tested using both conventional single stage tests, as well as multistage triaxial tests. In these multistage tests the deflection point of the volumetric strain curve, $\frac{d\varepsilon_{vol}}{d\sigma} = 0$, is used as a termination point. Following this method, no premature sample failure occurred. The failure envelope and other mechanical properties specifically Young's modulus, E, and Poisson's ratio, $\nu$, obtained from a multistage test are compared to those obtained from single stage conventional test. The stress at which the test is ceased in each loading stage is easy to pick and guarantees the integrity of the sample. Furthermore the plug experiences minimum alteration of its mechanical properties, as it is never stressed far beyond the elastic region. The data acquired from this test can be used to construct a complete failure envelope from a single sample.

### 5.1.2 Methodology

### 5.2.1 Picking the stress termination point

An impediment to obtaining meaningful results from a multistage test is identifying the stress at which the test should be stopped. The termination stress most widely used by researchers is that of "a sample exhibiting failure." Kovari and Tisa (1975) showed that the peak strength obtained in multistage tests using this point is negligibly different than the peak strength obtained from single stage tests. This result justified the use of this criterion in a number of studies. However, there is no doubt that this point is not easily identifiable during the test. Additionally, irreversible mechanical changes take place in the samples after experiencing these stress magnitudes and consequently this method was abandoned and not used in this study.

The next criterion evaluated was stopping the axial load when the volumetric strain becomes zero. Samples can and have failed before reaching this requirement (Figure 5.1). Furthermore, we observed that during the single stage tests at different confining pressures, the difference between the stresses when at $\varepsilon_{vol}= 0$ and the actual failure stress is confining pressure dependent (Figure 5.2). Failure envelopes constructed from this termination stress criterion will systematically be raised by the pressure dependence shown on Figure 5.2. For high confining pressures this stress is close to the actual failure stress whereas for low confining pressures the difference between the two stresses is large. This will

result in a failure envelope line with a steeper slope (larger $\phi$), hence smaller value for C.

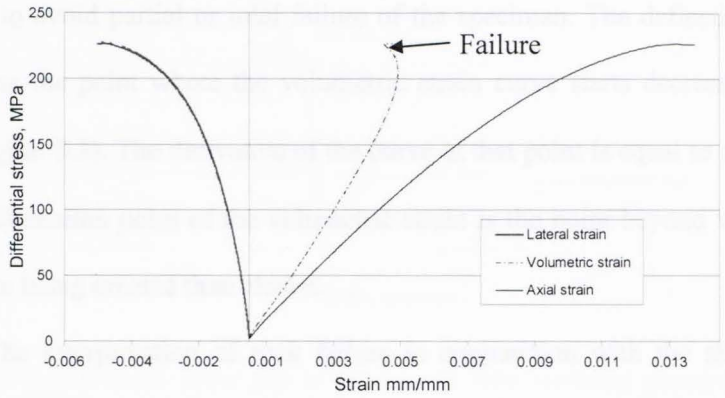


**Figure 5.1 Applied axial stress versus strains for sample H8. Plotted are the measured axial and lateral strains and the computed volumetric strain. Obviously using the criterion of stopping the test when the volumetric strain becomes zero would be inapplicable as the sample failed before this point could be reached.**

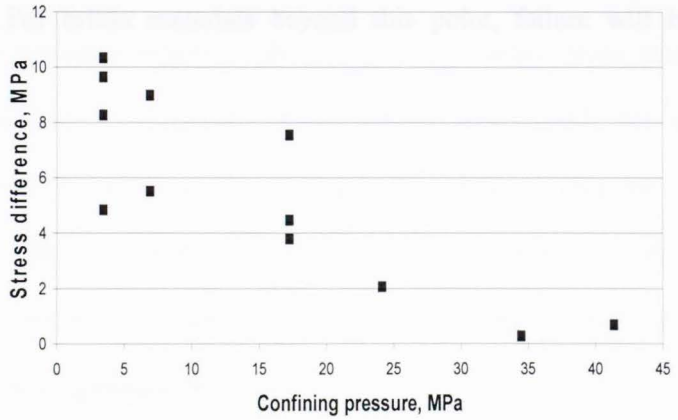


**Figure 5.2 Confining pressure dependency of the pressure difference between the stresses at the point where the volumetric strain is equal to zero and the failure stress. These data were obtained from single stage tests on Berea sandstone.**

In this study, the deflection point on the volumetric strain curve was evaluated as the termination point at each confining pressure. This point is selected to avoid partial or total failure of the specimen. The deflection point is defined as the point where the volumetric strain curve starts decreasing after a peak (Figure 5.3). The derivative of the curve at that point is equal to zero ($\varepsilon'_{vol} = 0$). The deflection point of the volumetric strain is the point beyond which more cracks are being created than closed.

The interpretation of rock failure in conjunction with the shape of the volumetric strain curve is presented in Figure 2.7. According to Bieniawski (1967), the point where the volumetric strain deflects marks the beginning of the stress state where the fracture has an unstable propagation and control of failure is difficult. For brittle materials beyond this point, failure will be sudden and eruptive.

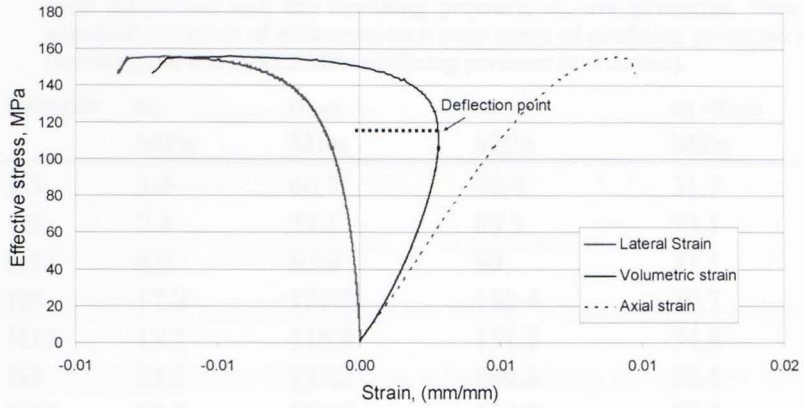


**Figure 5.3 Typical stress strain plot of Berea (17.2 MPa confining pressure) where the deflection point of the volumetric strain is indicated.**

The deflection point however, is not an arbitrary point and is intimately related to failure. It has a uniform deviation from the failure point for different confining pressures which is shown in data obtained from single stage tests detailed in Table 5.1. This difference is almost constant with very small variations (Figure 5.4). In an effort to investigate the physical meaning of those small variations, they were plotted against different rock properties such as mineralogy, porosity, permeability and so on but no meaningful relationships could be observed (see Appendix III).

Table 5.1 Single stage triaxial test results. Stresses at the deflection point, $\sigma_{defl}$ failure, $\sigma_f$ their differences and the confining pressure, $\sigma_c$, are presented. Note that the standard deviation of difference on a wide range of confining pressures is 6% not including the test at 55.2 MPa confining pressure (not shown).

| Sample | $\sigma_c$ | $\sigma_{defl}$ | $\sigma_f$ | $\sigma_f - \sigma_{defl}$ |
|---|---|---|---|---|
| | MPa | MPa | MPa | MPa |
| **H3** | 3.4 | 60.7 | 92.4 | 31.7 |
| **H6** | 3.4 | 55.1 | 88.3 | 33.1 |
| **H14** | 6.9 | 65.9 | 99 | 33.1 |
| **H5** | 17.2 | 121.7 | 152.4 | 30.7 |
| **H12** | 17.2 | 116.9 | 151.7 | 34.8 |
| **H9** | 24.1 | 137.2 | 169.3 | 32.1 |
| **H10** | 34.5 | 156.2 | 189.7 | 33.5 |
| **H13** | 34.5 | 161 | 190 | 29 |
| | | **Average** | | **32.2** |
| | | **Standard Deviation** | | **1.8** |
| | | **Error** | | **5.6%** |

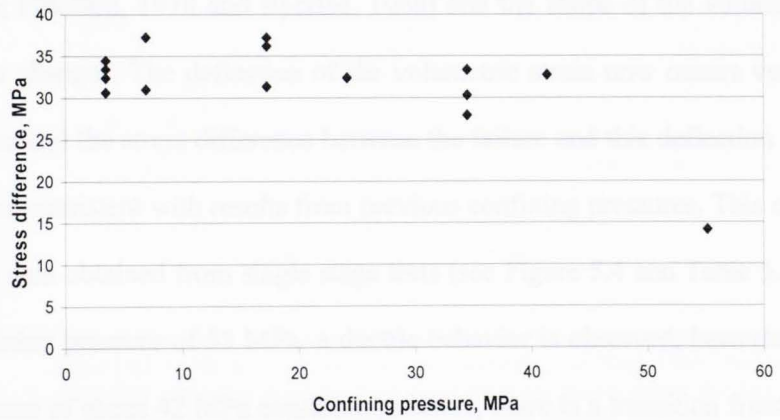


Figure 5.4 Pressure dependence of the stress difference between the failure and the deflection of the volumetric strain. Note that at the confining pressure of 55 MPa the point does not follow the trend and is not included in Table 5.1.

This average difference between the failure and deflection stresses is 32.24 ± 1.82 MPa. This is a variation of less than 6%. We can therefore construct a failure envelope based on the stresses at the deflection points which will be nearly parallel to the one constructed from failure stresses. It will be parallel as a result of the consistency of the difference in stresses between the failure point and the deflection point for all the confining pressures below 42 MPa. This information can be obtained before reaching the strength limit of the sample so there is no need to know *a priori* the behavior of the failure curve in order to have meaningful results. There is a limitation however, the test has to be performed under low enough confining pressures to allow brittle failure of the sample. At very high confining pressures, the sample fails plastically (Mogi, 1966; Paterson, 1978 and Byerlee, 1968) and the shape of the volumetric strain curve changes. The deflection of the volumetric strain now occurs very close to failure and the stress difference between the failure and this deflection point is no longer consistent with results from previous confining pressures. This can be seen from data obtained from single stage tests (see Figure 5.4 and Table 5.6a). At the confining pressure of 55 MPa, a ductile behavior is observed, because above the pressure of about 42 MPa confining pressure, there is a transition from the brittle to the ductile region due to confining pressure. The transition is described by Byerlee (1968) and Mogi (1966) and is discussed in Chapter 2 (see Figure 2.8). Failure stress data from the samples used in this study are plotted in a differential

stress-confining pressure space (Figure 5.5) along with the two transition lines as described by Byerlee (1968) and Mogi (1966). Mogi's line intercepts the results of this study at the confining pressure of 42 MPa suggesting that this is the confining pressure above which the rock behaves ductily. This pressure is in accord with other studies on Berea sandstone. However, Byerlee's line would place the transition near 10 MPa, clearly inconsistent with our observations. Byerlee's transition line does not describe the phenomenon well for low confining pressures (see Figure 2.8) or for porous rocks.

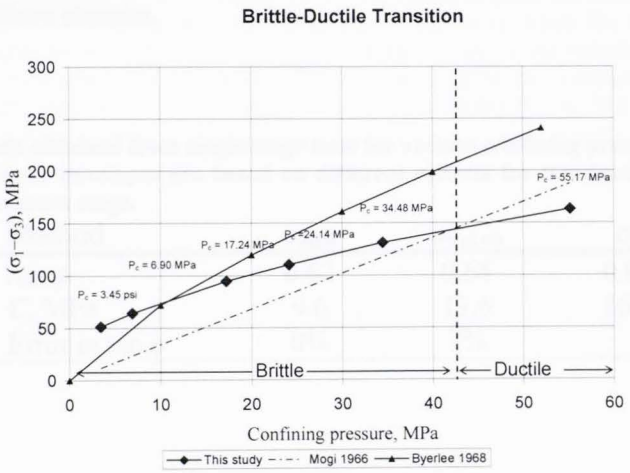


**Figure 5.5 Plot of the shear failure stress for different confining pressures and the line that separates brittle and ductile behavior according to Mogi 1966. Points lying in the area above the line show brittle failure whereas points below the line show ductile failure. Byerlee's (1968) transition line is also plotted. However, this line does not describe the transition observed in this study.**

Using the data obtained from single stage tests at different confining pressures, we can obtain three different failure envelopes (Figure 5.6). The first

line is constructed using stresses at the deflection point of the volumetric strain, the second using stresses at the point where the volumetric strain is equal to zero and a third from the actual failure values (Table 5.2). The comparison of these lines shows that the failure envelope constructed from the deflection point stresses has almost the same inclination (***tan*** $\phi$) as the failure envelope based on conventional tests. Note that these results are before shifting. The large difference in the C term results from not properly shifting the failure envelope. In contrast the second failure envelope has an error of 7% compared to the failure envelope from the failure stresses.

**Table 5.2 Data obtained from single stage tests for various confining pressures. The different failure envelopes are based on different criteria for terminating the test at each pressure stage.**

| Method | $\sigma_{defl}$ | $\sigma_{vol.=0}$ | $\sigma_f$ |
|---|---|---|---|
| *tan* $\phi$ | 0.62 | 0.64 | 0.62 |
| ***C***, MPa | 9.6 | 13.6 | 16.1 |
| Error in tan $\phi$ | 0% | 7% | |

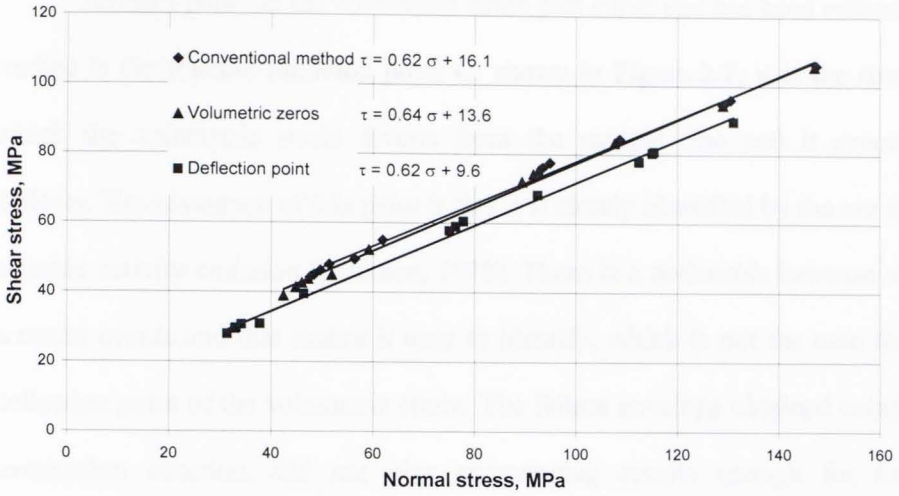


**Figure 5.6 Comparison between failure envelopes obtained from the three stress termination criteria (1) stress at failure (diamonds), (2) stress when the volumetric strain is equal to zero (triangles) and (3) deflection point of the volumetric strain (boxes). It is obvious that the envelope corresponding to the volumetric strain equal to zero criteria is not comparable to the conventional one. The equations describe the Mohr's failure criterion are of the form: $\tau = \tan\phi\ \sigma + C$.**

The deflection point of the volumetric strain is easy to pick thus minimizing operator subjectivity. Depending on how ductile the rock is, there can be a wide range of stresses that may fit the characterization "sign of failure". Stress values when the volumetric strain reaches its greatest value and starts decreasing, can be easily identified while performing the test. During the test, the volumetric strain keeps increasing. It is fairly easy to identify a plateau after which the volumetric strain starts decreasing. That is the point where loading is terminated. However, the operator has the ability of even passing that point without risking failure.

Another point on the volumetric strain plot curve that has been extensively studied is the fracture initiation point C' shown in Figure 2.7; it is the stress at which the volumetric strain diverts from the straight line and it eventually deflects. The advantage of this point is that it is clearly identified by the use of the acoustic activity emission (Paterson, 1978). There is a noticeable increase of the acoustic events and that makes it easy to identify, which is not the case for the deflection point of the volumetric strain. The failure envelope obtained using this termination criterion, did not give encouraging results enough for further investigation. There is confining pressure dependence between this point and the actual failure and it does not yield a predictable trend. However, acoustic activity emission may give better results than what one can get by a simple visual inspection of the volumetric strain.

### 5.2.2 Multistage process

Tests were conducted in a servo-controlled hydraulic press MTS-215. Two extensometers mounted on the sample measure axial and circumferential displacements. The test procedure is as follows:

1. The confining pressure is increased to the first pressure stage while the differential axial load is kept at a zero (There is a minimum load to verify that the ram is always in contact with the sample). At that point the displacement gages are zeroed and data acquisition initiates.

2. Axial load increases at constant confining pressure and fixed strain rate, $\dot{\varepsilon} \approx 10^{-6}$. Axial and lateral strain, are recorded whereas volumetric strain is calculated. All three strains are plotted continuously during the test.
3. Loading is stopped at the deflection point of the volumetric strain curve.
4. The axial load is slowly decreased to hydrostatic condition. Again it is very important to maintain the differential positive stress ($\sigma_1$-$\sigma_3$) close to zero but not negative. That assures that the piston touches the sample so it will not move from its position and the confining fluid will leak into the sample.
5. The pressure is increased hydrostatically to a new confining pressure value.
6. The procedure described in steps 2 through 5 is repeated for as many pressure stages as required.

In the last pressure stage the sample is brought to failure yielding information about the failure strength at that confining pressure. This procedure is described in the stress path shown in Figure 5.7 while Figure 5.8 gives a complete stress – strain plot for sample **H26**.

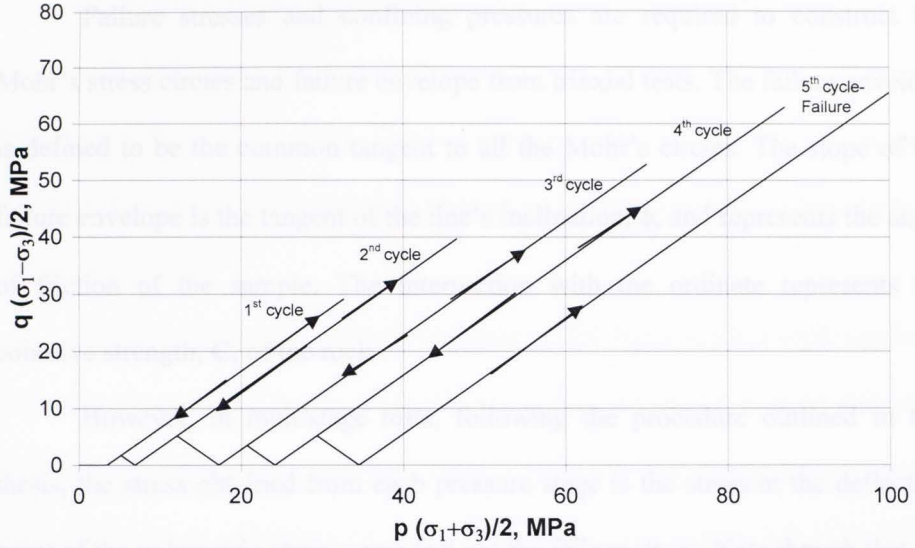


**Figure 5.7 Complete stress path for a multistage test in q-p space.**

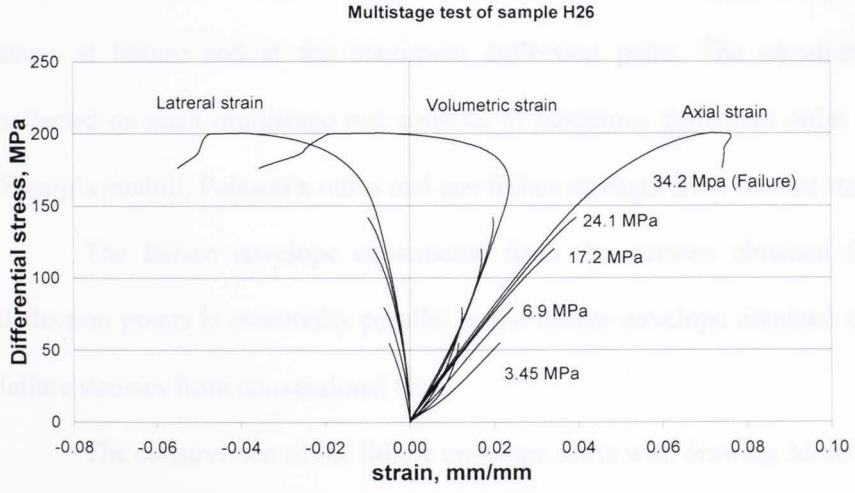


**Figure 5.8 Complete multistage test for sample H26. The confining pressure of each stage is shown next to the axial strain curve. Failure takes place at the last confining pressure (34.2 MPa).**

### 5.1.3 Construction of the failure envelope

Failure stresses and confining pressures are required to construct the Mohr's stress circles and failure envelope from triaxial tests. The failure envelope is defined to be the common tangent to all the Mohr's circles. The slope of the failure envelope is the tangent of the line's inclination, $\phi$, and represents the angle of friction of the sample. The intersection with the ordinate represents the cohesive strength, **C**, of the rock.

However, in multistage tests, following the procedure outlined in this thesis, the stress obtained from each pressure stage is the stress at the deflection point of the volumetric strain curve and not the failure stress. Note though that the sample is brought to failure on the last confining pressure stage; this yields both stress at failure and at the maximum deflection point. The cumulative data collected on each multistage test consists of numerous deflection point stresses, Young's moduli, Poisson's ratios and one failure strength from the last stage.

The failure envelope constructed from the stresses obtained from the deflection points is essentially parallel to the failure envelope obtained using the failure stresses from conventional tests.

The construction of the failure envelope starts with drawing Mohr's circles for the stress conditions for each stage, using the stresses at the deflection points. A tangent to these circles defines the failure envelope. This envelope is parallel to, but lower than the failure envelope based on failure stresses. Using the failure

strength determined during the last pressure stage we construct another Mohr's circle which has a common minimum normal stress but a larger radius. The first circle ends at the stress of the deflection point and the second ends at the stress of failure (see Figures 5.9a, 5.9b). The next step is to shift the deflection point based failure envelope so that it becomes tangent to the second circle made using the failure stress.

Another way to describe this process is that the stresses at each confining pressures are corrected by the stress difference between the stress at the deflection and failure obtained from the last confining pressure. The difference has already been shown to be confining pressure independent (see Figure 5.4). The values obtained from this procedure for cohesive strength, C, and the angle of failure, $\phi$, are presented in the next chapter.

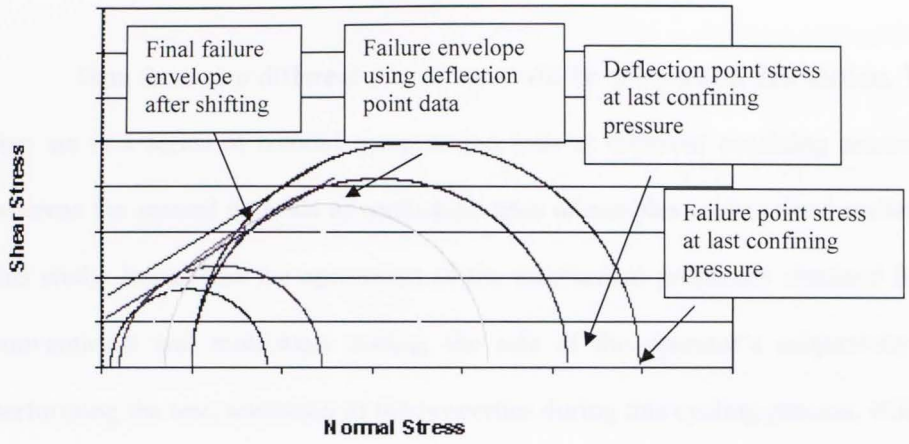


**Figure 5.9a Final failure envelope obtained from multistage tests. The lower failure envelope is drawn based on stresses at the deflection point of the volumetric strain. Shifting this failure envelope to be tangent to the Mohr's circle made in the last stage; the final failure envelope is obtained.**

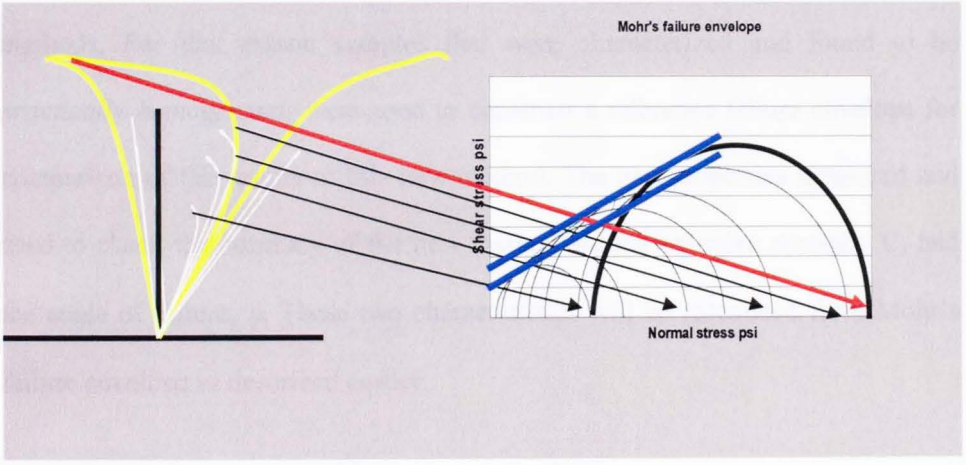


**Figure 5.9b Graphical presentation of Mohr's failure envelope construction using data from a multistage test.**

### 5.1.4 Data Analysis

Data from two different sets of tests will be analyzed in this section. The first set is a series of triaxial compression tests at different confining pressures whereas the second consists of multistage tests of samples as described earlier in this study. Issues like the agreement of the mechanical properties obtained from conventional and multistage testing, the role of the operator's subjectivity in performing the test, alteration of the properties during this cycling process, will be analyzed in this chapter.

The main goal of the multistage test is to give results totally comparable to those obtained conventionally with the existing expensive and time consuming methods. For that reason samples that were characterized and found to be *practically homogeneous* were used to construct a reference failure envelope for comparison of the results of this new method. The two properties measured and used to check the accuracy of the new method are the cohesive strength, C, and the angle of failure, $\phi$. These two characteristics will be calculated from Mohr's failure envelope as described earlier.

#### 5.1.4.1 Single stage results

As a first step we calculate the error that the samples characterized as *homogeneous* give when constructing the failure envelope.

Analyzing the data from 13 Berea sandstone samples tested at five different confining pressures (3.45, 6.9, 17.21, 24.14, 34.18 MPa), a common conventional failure envelope was defined. This failure envelope is best described by the equation $\tau_n = 0.62\sigma_n + 16.1$ where $\tau_n$ and $\sigma_n$ are in MPa. Heterogeneity is responsible for an estimated uncertainty of ± 7% in the cohesive strength and 2% in the angle of friction (see Table 5.3). These errors were calculated from the scatter in the single stage test data used in constructing the failure envelope.

**Table 5.3 Failure stresses obtained from single stage tests for various confining pressures. The error in *C* is 7% where as the error in *tan* $\phi$ is 2%.**

| Sample # | $\sigma_{conf}$ MPa | Shear MPa | Normal MPa |
|---|---|---|---|
| H3 | 3.45 | 46.21 | 49.66 |
| H6 | 3.45 | 44.14 | 47.59 |
| H24 | 3.45 | 47.93 | 51.38 |
| H25 | 3.45 | 45.01 | 48.46 |
| H14 | 6.90 | 49.50 | 56.39 |
| H21 | 6.90 | 55.00 | 61.90 |
| H5 | 17.24 | 76.21 | 93.45 |
| H12 | 17.24 | 75.86 | 93.10 |
| H23 | 17.24 | 77.59 | 94.83 |
| H9 | 24.14 | 84.48 | 108.62 |
| H10 | 34.48 | 94.48 | 128.97 |
| H13 | 34.48 | 94.62 | 129.10 |
| H22 | 34.48 | 96.02 | 130.51 |
| **Failure Envelope** | | | |
| | **C** | **tan $\phi$** | |
| **Average** | 0.62 | 16.10 | |
| **STDV** | 0.01 | 1.20 | |
| **Error** | 2% | 7% | |

These results are in agreement with previously reported values summarized in Table 5.4. and data is plotted in Figure AIII.6.

Table 5.4 Summary of reported mechanical data results for Berea sandstone.

| Author | $\sigma_{conf}$ | $\sigma_f$ | Author | $\sigma_{conf}$ | $\sigma_f$ |
|---|---|---|---|---|---|
| | | | This | | |
| Handin et al, | 0 | 70 | work | 0 | 46 |
| 1963 | 25 | 165 | | 3.45 | 96 |
| | 50 | 221 | | 3.45 | 92 |
| | 100 | 347 | | 3.45 | 99 |
| | 150 | 491 | | 3.45 | 93 |
| | 200 | 625 | | 6.9 | 106 |
| Wilhelmi and | 0 | 57 | | 6.9 | 117 |
| Somerton, | 3 | 114 | | 6.9 | 170 |
| 1967 | 7 | 145 | | 17.24 | 169 |
| | 14 | 188 | | 17.24 | 172 |
| | 28 | 259 | | 24.14 | 193 |
| Aldritch, | 0 | 68 | | 34.48 | 223 |
| 1969 | 7 | 120 | | 34.48 | 224 |
| | 21 | 178 | | 34.48 | 227 |
| | 34 | 220 | | 41.4 | 253 |
| | 55 | 252 | | 55.2 | 282 |
| Bernabe and | 10 | 116 | | | |
| Brace, | 50 | 227 | | | |
| 1990 | 90 | 226 | | | |
| | 130 | 282 | | | |

### 5.1.4.2 Multistage results

Multistage tests were run on four samples. The tests were stopped at the deflection point of the volumetric strain (Figure 5.10) and these stresses were used to construct the failure envelope. This constitutes the first step of the proposed construction method of a failure envelope.

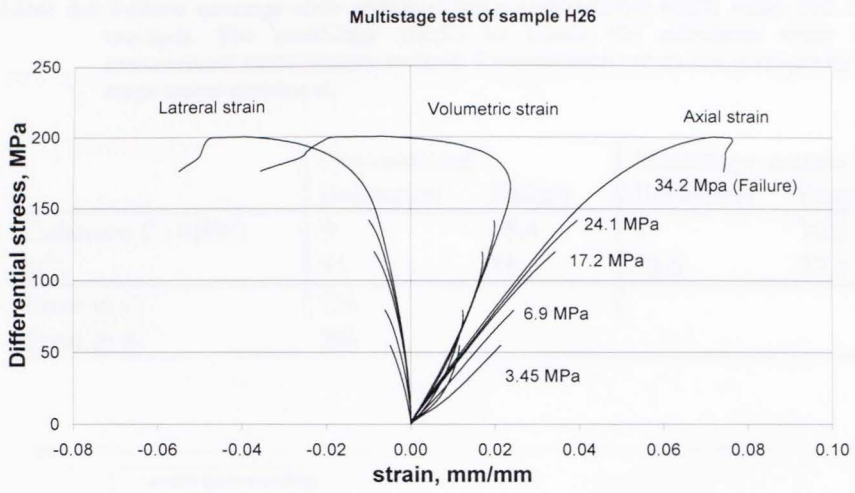


**Figure 5.10 Complete multistage test. The confining pressure of each stage is shown next to the axial strain curve. At the last confining pressure (34.2 MPa) failure takes place.**

Having established the errors for the standard method, we can proceed in calculating and comparing the failure envelopes obtained from the multistage tests. Table 5.6 presents the results of such a comparison. The first column of this table provides the information derived from the failure envelope produced from conventional testing using the deflection point stresses ($\boldsymbol{C}$ = 9 MPa, $\phi$ = 31°), and the failure stresses ($\boldsymbol{C}$ = 15.4 MPa, $\phi$ = 31°), respectively. The second column describes the failure envelope obtained using the maximum deflection of the volumetric strain criterion for sample **H26** before ($\boldsymbol{C}$ = 9 MPa, $\phi$ = 32.6°) and after ($\boldsymbol{C}$ = 14.8 MPa, $\phi$ = 32.6°) shifting the envelope (also see Figure 5.11).

**Table 5.5 Failure envelope data obtained from conventional single stage and multistage methods. The multistage results lie within the calculated error from the conventional multi-sample method. Conventional values are averages for all single stage tested specimens.**

| | Conventional | | Multistage sample H26 | |
|---|---|---|---|---|
| | Deflection | Failure | Deflection | Projected |
| Cohesion C (MPa) | 9 | 15.4 | 9 | 14.8 |
| $\phi(^{o})$ | 31 | 31 | 32.6 | 32.6 |
| Error in C | 7% | | | |
| Error in $\phi$ | 2% | | | |

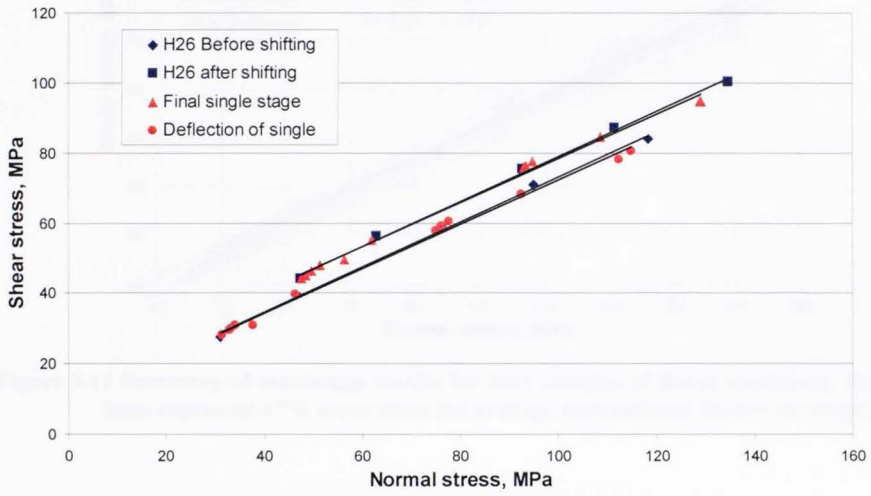


**Figure 5.11 Failure envelope data obtained from conventional single stage and multistage methods for sample H26. For both cases two different termination criteria where used.**

The failure envelope produced by the multistage test is comparable to the failure envelope obtained by the conventional testing method (see Figure 5.11) and most important the difference lies within the error margins calculated from the single stage test data. These error margins represent the variation of

mechanical properties due to sample heterogeneity. Failure envelopes obtained from multistage tests lie within the error bounds defined by the two dashed lines in Figure 5.12.

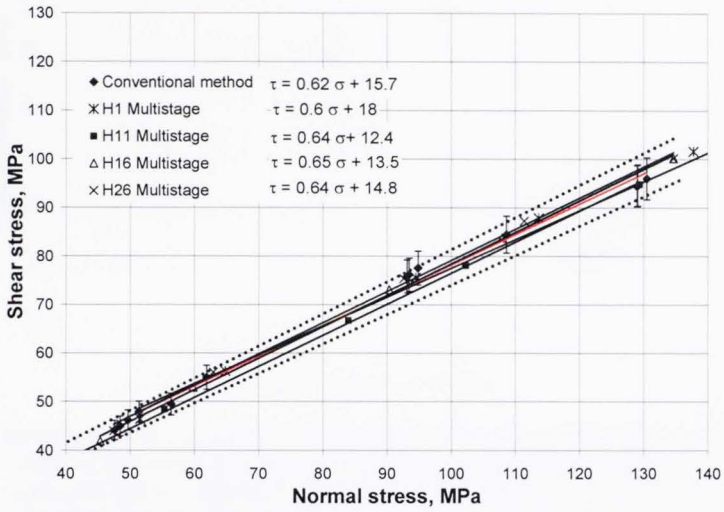


**Figure 5.12 Summary of multistage results for four samples of Berea sandstone. The dotted lines represent ±7% error from the average conventional failure envelope.**

### 5.1.4.3 Compressional and shear waves velocity

The dynamic Young's modulus, $E_D$, was also calculated from compressional and shear waves measured on companion plugs. The comparison of static with dynamic moduli is poor at low confining pressures and quite good at higher confining pressures (see Figure 5.13). This suggests the differences between dynamic and static moduli are largely driven by cracks. Cracks make the

rock nonlinear making direct comparisons unreasonable (Guyer and Johnson, 1999).

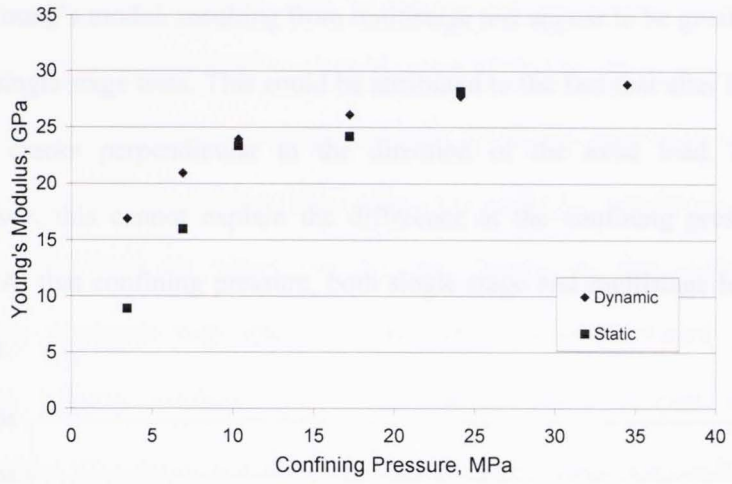


**Figure 5.13 Comparison between static, E, and dynamic Young's moduli, $E_D$. Note that static measurements of *E* were conducted at an axial load equal to the confining pressure which simulated the hydrostatic conditions of the dynamic experiment. Dynamic moduli are generally greater; the difference decreases with increasing confining pressure suggesting it is largely crack driven.**

### 5.1.4.4 Static Young's modulus and Poisson's ratio

The Young's moduli, ***E***, obtained from the multistage tests yield the expected trend when plotted against the confining pressure; **E** increased as the confining pressure increased. A logarithmic trend is observed and described by the equation;

$$E = 1.97 \ln(\sigma_c) + 19.23 \quad \text{.....(5.1)}$$

where E is in GPa and $\sigma_c$ in MPa

In contrast, the trend obtained by using the conventional testing method, does not follow the expected trend. Sample heterogeneity is responsible for the observed scatter. In Figure 5.14, ***E*** has been plotted against confining pressure. The Young's moduli resulting from multistage test appear to be greater than those from single stage tests. This could be attributed to the fact that after the first cycle small cracks perpendicular to the direction of the axial load, have closed. However, this cannot explain the difference at the confining pressure of 3.45 MPa. At that confining pressure, both single stage and multistage have not been cycled.

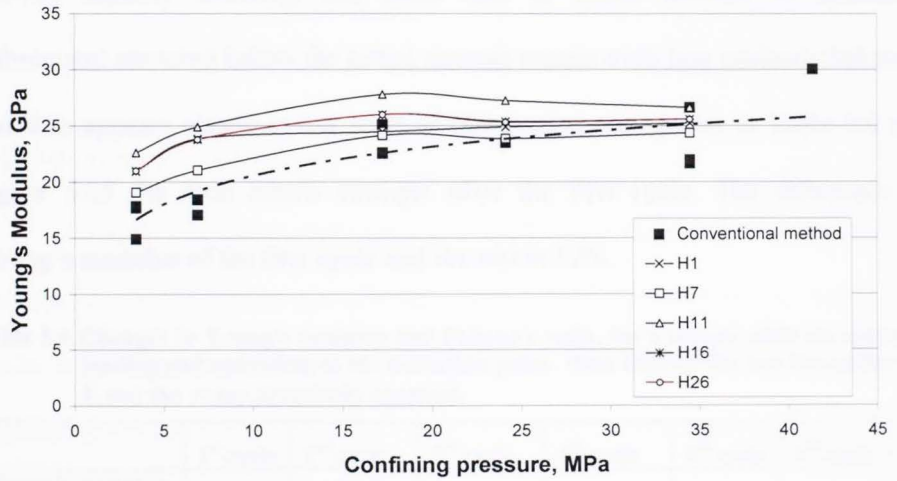


**Figure 5.14 Young's modulus measured from conventional (closed boxes) and multistage tests. Note that the single stage test values display greater dispersion. The dashed line is the logarithmic trend-line for the conventional tests.**

### 5.1.4.5 Cycle Test

Another test performed in this study, was the cycling of a sample at a constant confining pressure. The results of this test indicate that the sample damage is small if the test is stopped at the deflection point of the volumetric strain. The Young's modulus measured after six cycles of loading and unloading at constant confining pressure (3.45 MPa) was practically unaltered. The only run that differed from the others was the first. During the first cycle, elastic and anelastic processes take place. The anelastic processes include minor crack growth, asperity crushing, etc; these lead to minor amount of hysterisis. Subsequent stressing below the initial stresses causes even less anelastic behavior and thus appears elastic at our scale of observation. As shown in Table 5.6 and Figure 5.15 the rock seems stronger after the first cycle. The difference in Young's modulus of the first cycle and the rest is 12%.

**Table 5.6 Changes in Young's modulus and Poisson's ratio, for a sample after six cycles of loading and unloading to the deflection point. Note that for the last five cycles the E and the ν stay practically constant.**

| | 1st cycle | 2nd cycle | 3rd cycle | 4th cycle | 5th cycle | 6th cycle |
|---|---|---|---|---|---|---|
| **Young's modulus E, (GPa)** | 20.5 | 22.7 | 23.1 | 23.3 | 23.1 | 23.4 |
| **Poisson's ratio, ν** | 0.20 | 0.20 | 0.20 | 0.21 | 0.20 | 0.24 |
| **$\sigma$ @ $\varepsilon_{vol}' = 0$** | 55.18 | 55.18 | 55.18 | 55.18 | 55.18 | 59.67 |
| **Strain rate ($*10^{-7}$)** | 8.36 | 3.21 | 2.21 | 1.97 | 1.39 | 1.22 |

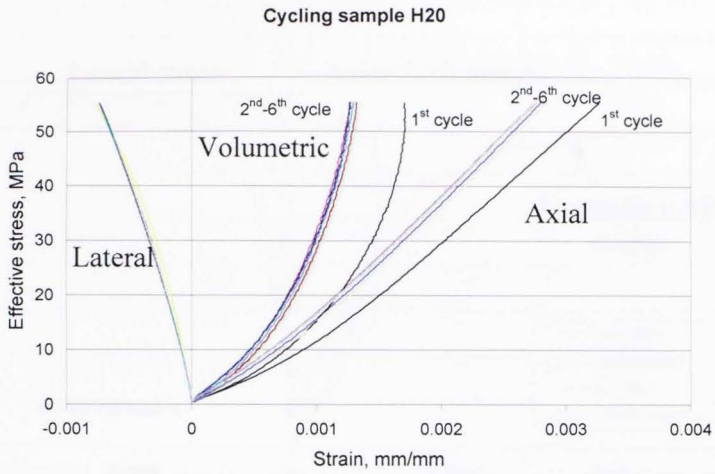


**Figure 5.15 Stress-strain plot showing the axial the lateral and the volumetric strains of the cycled sample H20. The cycle ends at the point where the volumetric strain deflects.**

## 5.1.4.6 Acoustic Emission

Acoustic emissions were also recorded during some tests. We observed an increase of the number of the acoustic events at the point where the volumetric strain starts deviating from its linear behavior. There is a small increase in the number of events at the deflection point (see Figure 5.16). However this point is difficult to define in real-time. Future work should investigate using AE to define the deflection point. Improvement in signal to noise may make AE a more viable approach

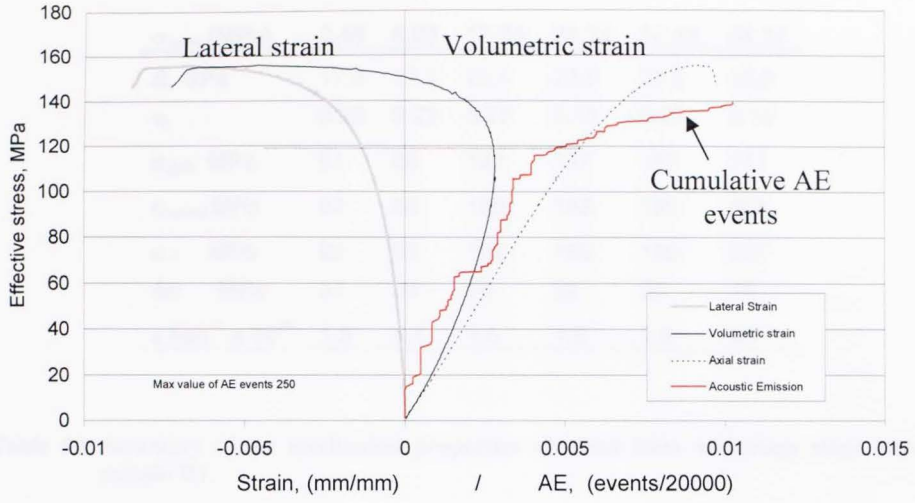


**Figure 5.16 Sample broken at 17.24 MPa. The red line is the number of acoustic emissions divided by 20,000. Note the change of the rate of activity at the deflection point.**

Table 5.7 Summary of the mechanical properties obtained from single stage tests.

| $\sigma_{conf}$ (MPa) | 3.45 | 6.90 | 17.24 | 24.14 | 34.48 | 55.17 |
|---|---|---|---|---|---|---|
| E, GPa | 17.8 | 17.2 | 22.5 | 23.6 | 23.9 | 25.5 |
| $\nu$, | 0.29 | 0.22 | 0.23 | 0.18 | 0.21 | 0.18 |
| $\sigma_{defl}$ MPa | 61 | 66 | 122 | 137 | 157 | 211 |
| $\sigma_{vol=0}$ MPa | 83 | 89 | 150 | 168 | 190 | N/A |
| $\sigma_f$ MPa | 92 | 99 | 152 | 169 | 190 | 227 |
| $\Delta\sigma$ MPa | 31 | 33 | 30 | 32 | 33 | 16 |
| $\varepsilon$ $sec^{-1}$ x $10^{-6}$ | 1.5 | 1.7 | 1.6 | 1.6 | 1.6 | 1.7 |

Table 5.8 Summary of the mechanical properties obtained from multistage stage tests of sample H1.

| $\sigma_{conf}$ (MPa) | 3.45 | 6.90 | 17.24 | 24.14 | 34.48 | 55.17 |
|---|---|---|---|---|---|---|
| E, GPa | 20.9 | 23.8 | 24.5 | 24.9 | 25.2 | 25.7 |
| $\nu$, | 0.25 | 0.29 | 0.27 | 0.24 | 0.23 | 0.22 |
| $\sigma_{defl}$ MPa | 63 | 84 | 124 | 148 | 178 | 225 |
| $\sigma_f$ MPa | N/A | N/A | N/A | N/A | N/A | 236 |
| $\varepsilon$ $sec^{-1}$ x $10^{-6}$ | 1.6 | 1.5 | 1.6 | 1.6 | 1.6 | 1.6 |

Table 5.9 Summary of mechanical petrophysical and stress observations during single stage tests.

| Sample | E | n | $\sigma_c$ | $\sigma_1$-$\sigma_3$ | $\sigma_f$ | $\sigma_{vol.=0}$ | $\sigma_{defl}$ | $\sigma_{C'}$ | Porosity | k |
|---|---|---|---|---|---|---|---|---|---|---|
| | GPa | | MPa | MPa | MPa | MPa | MPa | MPa | % | mD |
| **H19** | 7.09 | 0.19 | 0.00 | 46.2 | 46.2 | 41.7 | 22.1 | 11.7 | 20.3 | 176 |
| **H3** | 17.82 | 0.28 | 3.45 | 92.4 | 95.9 | 82.8 | 59.0 | 32.8 | 19.1 | 150 |
| **H6** | 17.83 | 0.30 | 3.45 | 88.3 | 91.7 | 77.9 | 55.9 | 24.5 | 19.1 | 146 |
| **H24** | 17.71 | 0.32 | 3.45 | 95.9 | 99.3 | 87.6 | 61.4 | 38.3 | 20.1 | 188 |
| **H25**** | 14.92 | 0.33 | 3.45 | 90.0 | 93.5 | 85.2 | 59.3 | 40.7 | | |
| **H14** | 17.08 | 0.20 | 6.90 | 99.0 | 105.9 | 90.0 | 61.7 | 26.9 | 19.6 | 176 |
| **H21** | 18.43 | 0.16 | 6.90 | 110.0 | 116.9 | 104.5 | 79.0 | 42.4 | 20.4 | 188 |
| **H5** | 22.55 | 0.23 | 17.24 | 152.4 | 169.7 | 148.6 | 121.0 | 60.3 | 19.2 | 167 |
| **H12** | 25.09 | 0.28 | 17.24 | 151.7 | 169.0 | 144.2 | 115.5 | 83.4 | 19.4 | 171 |
| **H23** | 22.59 | 0.14 | 17.24 | 155.2 | 172.4 | 150.7 | 118.0 | 78.0 | 20.2 | 172 |
| **H9** | 23.51 | 0.19 | 24.14 | 169.0 | 193.1 | 166.9 | 136.6 | 67.2 | 19.3 | 171 |
| **H10** | 21.67 | 0.20 | 34.48 | 189.0 | 223.4 | 189.0 | 161.0 | 140.4 | 19 | 147 |
| **H13** | 21.96 | 0.19 | 34.48 | 189.2 | 223.7 | 189.0 | 155.9 | 141.4 | 19.9 | 176 |
| **H22** | 26.63 | 0.12 | 34.48 | 192.0 | 226.5 | 0.0 | 161.7 | 135.9 | 20.5 | 188 |
| **H27**** | 30.04 | 0.18 | 41.38 | 212.1 | 253.4 | 211.4 | 179.3 | 141.0 | | |
| **H8** | 25.48 | 0.18 | 55.17 | 226.6 | 281.7 | 0.0 | 212.4 | 153.4 | 19.5 | 174 |

Table 5.10 Summary of mechanical petrophysical and stress observations during of multistage tests.

| Sample | E | ν | $\sigma_c$ | $\sigma_{defl.}$ | $\sigma_f$ | Projected $\tau_n$ | Projected $\sigma_n$ | Porosity | k |
|---|---|---|---|---|---|---|---|---|---|
| | GPa | | MPa | MPa | MPa | MPa | MPa | % | mD |
| **H1a** | 20.94 | 0.25 | 3.45 | 63.1 | | 46.4 | 51.6 | 19.4 | 148 |
| **H1b** | 23.83 | 0.29 | 6.90 | 82.8 | | 56.3 | 64.8 | | |
| **H1c** | 24.47 | 0.27 | 17.24 | 121.4 | | 75.6 | 94.5 | | |
| **H1d** | 24.90 | 0.24 | 24.14 | 145.9 | | 87.9 | 113.6 | | |
| **H1e** | 25.23 | 0.23 | 34.48 | 173.5 | | 101.6 | 137.8 | | |
| **H1f** | 25.74 | 0.22 | 55.17 | 220.7 | 16.6 | 118.6 | 173.8 | | |
| **H7a** | 19.07 | 0.29 | 3.45 | 46.9 | | 38.4 | 41.9 | 18.6 | 101 |
| **H7b** | 21.05 | 0.27 | 6.90 | 66.9 | | 48.4 | 55.3 | | |
| **H7c** | 24.15 | 0.21 | 17.24 | 103.4 | | 66.7 | 84.0 | | |
| **H7d** | 23.86 | 0.20 | 24.14 | 126.2 | | 78.1 | 102.2 | | |
| **H7e** | 24.36 | 0.15 | 34.48 | 159.7 | 30.0 | 94.8 | 129.3 | | |
| **H11a** | 22.61 | 0.28 | 3.45 | 48.6 | | 38.4 | 41.9 | 19.5 | 172 |
| **H11b** | 24.90 | 0.32 | 6.90 | 69.0 | | 48.6 | 55.5 | | |
| **H11c** | 27.78 | 0.28 | 17.24 | 103.8 | | 66.0 | 83.3 | | |
| **H11d** | 27.23 | 0.26 | 24.14 | 126.6 | | 77.4 | 101.6 | | |
| **H11e** | 26.62 | 0.24 | 34.48 | 163.8 | 28.3 | 96.0 | 130.5 | | |
| **H16a** | 20.99 | 0.23 | 3.45 | 53.1 | | 41.9 | 45.3 | 19.8 | 173 |
| **H16b** | 23.76 | 0.19 | 6.90 | 75.2 | | 52.9 | 59.8 | | |
| **H16c** | 25.97 | 0.14 | 17.24 | 115.5 | | 73.1 | 90.3 | | |
| **H16d** | 25.36 | 0.13 | 24.14 | 136.9 | | 83.8 | 107.9 | | |
| **H16e** | 25.57 | 0.12 | 34.48 | 169.7 | 30.7 | 100.2 | 134.7 | | |
| **H26a**** | 21.00 | 0.23 | 3.45 | 55.2 | | 44.0 | 47.4 | | |
| **H26b** | 23.76 | 0.19 | 6.90 | 79.3 | | 56.0 | 62.9 | | |
| **H26c** | 25.97 | 0.14 | 17.24 | 117.9 | | 75.4 | 92.6 | | |
| **H26d** | 25.31 | 0.13 | 24.14 | 141.7 | | 87.3 | 111.4 | | |
| **H26e** | 25.57 | 0.12 | 34.48 | 167.6 | 32.8 | 100.2 | 134.7 | | |

# Chapter 6

## 6.1 Summary

A new method of performing multistage tests is suggested and evaluated. The goal of the study is to develop a repeatable multistage triaxial testing technique which will yield the failure envelope and values of Young's modulus and Poisson's ratio at different confining pressures from a single core plug. It also has to be a non-destructive technique so there will be no risk of uncontrolled failure before the completion of the test. Furthermore there should be no measurable alteration of the mechanical properties after each loading stage.

For this purpose two series of tests were performed on samples from the same block of Berea sandstone. The first tests in the series were conventional single stage tests. These gave the reference failure envelope for comparison with the multistage tests. The second series of tests were multistage tests.

Different criteria to stop the loading at each confining pressure were evaluated. It is clear that the volumetric strain curve is a much more useful in defining criterion for terminating load than the axial strain curve. The volumetric strain curve is more sensitive to stress changes prior to failure, giving more insights about the stressed rock. In addition, the Berea sandstone has a very repeatable behavior with easy to distinguish stages of deformation. The criterion of the deflection point, gives the exact same angle of friction as the conventional

method and after proper shifting, yielding cohesive strength values in agreement with the conventionally obtained values.

Using existing multistage techniques which depend on the operator's ability to recognize the peak strength of the rock before failure results in large errors in the calculation of the failure envelope characteristics (up to 35%; Kim and Ko, 1979). The largest errors were encountered for brittle materials. Brittle failure is often sudden and uncontrollable. Operators, tend to terminate the test prematurely, fearing failure, yielding stress values far below true failure values.

For comparison purposes, a failure envelope was constructed from single stage tests. This failure envelope can be described by a single equation:

$$\tau = 0.62\sigma + 15.7 \quad (6.1)$$

where $\tau$ and $\sigma$, all in MPa.

Statistical analysis of the linearity of this equation yields two error estimates for the angle of friction ±2% and for the cohesion ±7%. These two values should bound the failure envelopes obtained from this multistage technique. The observed resulting failure envelopes using the new technique do not fall far the error estimated for single stage tests.

The equations that describe failure envelopes obtained from the four multistage tests are summarized in table 6.1.

Table 5.1 summarizes all the multistage tests and conventional test results. Note the errors of the internal friction and the cohesive strength do not exceed the

error initially calculated from the single stage tests. This error is far less than any of the measurements for tests using previously defined multistage techniques.

**Table 6.1 Summary of failure envelope parameters derived from the present multistage technique and those from single stage tests.**

| Sample | Equations | Angle of friction Degrees | Cohesion MPa |
|---|---|---|---|
| H1 | $\tau = 0.60\sigma + 18.0$ | 31 | 18 |
| H11 | $\tau = 0.64\sigma + 12.4$ | 33 | 12.4 |
| H16 | $\tau = 0.65\sigma + 13.5$ | 33 | 13.5 |
| H26 | $\tau = 0.64\sigma + 14.8$ | 33 | 14.8 |
| Average | | 32 | 14.7 |
| STDev | | 1 | 2.4 |
| Single stage | | 32 | 15.7 |

AE were also recorded in an effort to evaluate additional objective ways of identifying and determining the deflection point of the volumetric strain. The results were encouraging. There was a change in the AE at the deflection point of the volumetric strain. However, this response of the AE could not be identified early enough to be useful for the purposes of this method. By the time the change in the trend of the AE became clear, the sample has experienced a large amount of stress and maybe too near its failure. Improvement in signal to noise may make AE a more viable approach.

The samples that were used for this study were petrophysically characterized. The result of this characterization showed these samples to be homogeneous. The observed variability in mechanical properties shows that

evidently, *homogeneous* is a term that we should be very cautious when using to characterize rock.

This comment leads to a second advantage of this method which is the total elimination of the issues of sample heterogeneity, since only one sample is required. Trends of the Poisson's ratio and Young's moduli plotted against confining pressure, obtained by multistage tests, show less scatter than those obtained the conventional way. Heterogeneity issues also affect the failure envelope causing large errors in calculating the angle of internal friction and the cohesive strength.

Finally, results of stress cycled samples, cycled at constant confining pressure until the deflection point of the volumetric strain, showed no detectable changes in the measured mechanical properties. Thus stopping the multistage test at the deflection point guarantees that the mechanical properties measured after the first cycle will not be affected by the earlier cycles. Results showed that excluding the first cycle, mechanical properties become quite repeatable for the remaining cycles.

## 6.2 Conclusions

The advantages of using the multistage method are:

- it eliminates heterogeneity issues making use of a single plug; and
- it is economically efficient maximizing the information obtained from a single plug.

The multistage method suggested in this thesis produces values for failure envelope characteristics **C** and $\phi$ from multiple-sample single stage tests. Additional advantages of this multistage technique compared to previously suggested multistage techniques are:

- it is not subjective using a distinctive point for terminating loading for each pressure stage;
- it guarantees no premature test terminations;
- it is repeatable for brittle rocks; and
- it gives minimal errors.

**Nomenclature**

$\mathbf{C}$ = cohesive strength
C' = onset of dilatancy
E = Young's modulus
$E_D$ = dynamic Young's modulus
$E_D$ = dynamic Bulk modulus
K = permeability
STDev = standard deviation
$\dot{\varepsilon}$ = strain rate, derivative of strain in respect of time
$\varepsilon_A$ = axial stain
$\varepsilon_L$ = lateral strain
$\varepsilon_{vol}$ = volumetric strain
$\phi$ = angle of internal friction
$\beta$ = the angle between that failure plane and the horizontal
$\nu$ = Poisson's ratio
$\nu_D$ = Dynamic Poisson's ratio
$\sigma_c$ = confining pressure
$\sigma_{defl}$ = stress at maximum inflection of volumetric strain curve
$\sigma_f$ = failure stress
$\sigma_n$ = stress on the failure plane
$\sigma_p$ = pore pressure
$\sigma_{vol=0}$ = stress at the point where the volumetric strain becomes zero
$\tau_n$ = shear stress on the failure plane

Conversion unit 1 MPa = 145.038 psi

* Core Laboratories Ltd.
** For these samples porosity and permeability was measured with a different apparatus and numbers do not match.

## References


1. Aldritch, M. J., Pore pressure effects on Berea sandstone subjected to experimental deformation., Geol. Soc. Amer. Bull. 1969, 80, 1577-1586
2. Bernabe, Y. and W. F. Brace, Deformation and fracture of Berea sandstone, in the Brittle-Ductile transition in rocks., Geophys. Mon. 1990, 56, 91-101
3. Bieniawski Z.T., Mechanism of Brittle failure of rock., Pretoria, South Africa: National mech. engineering research institute, Counsil, 1967
4. Birch, F., Compressibility; elastic constants, in Handbook of Physical Constants., edited by S. P. Clark, Jr., Geol. Soc. Amer. Memoir 1966, 97, 107-173
5. Brace W. F., Paudling W. B. Jr. and C. Scholz, Dilactancy in the fracture of crystalline rocks., Geophys. Res. 1966, 71, no 16, pp 3939- 3953
6. Bro A., Analysis of multistage triaxial test results for a strain-hardening rock., Int. J. Rock Mechanics and Min. Sci., 1997, 34, 143-145
7. Byerlee J. D., Brittle-ductile transition in rock., Geophys. Research, 1968, 73, 14, 4741-4750
8. Byerlee J. D., Friction of rocks., PAGEOPH, 1978, 116, 615-626

9. Crawford A. and D. Wylie, A modified multiple failure state triaxial testing method., 28th US Symposium on Rock Mechanics, 1987, 133-140
10. Guyer R. A. and A. P. Johnson, Nonlinear mesoscopic elasticity: evidence for a new class of materials., Physics Today, April 1999, 30-36
11. Handin J., Hager, R. V., Friedman, M. and J.N. Feather, Experimental deformation of sedimentary rocks under confining pressure: Tests at room temperature on dry samples., Bull. AAPG, 1963, 41, 1-50
12. Harouaka A., B. Mtawaa, A. Al-Majed, A. Abdulraheem and T. Klimentos, Multistage triaxial testing of actual reservoir cores under simulated reservoir conditions., Soc. Of Core Analysts, 1995,conference paper num. 9528, 1-9
13. Hawkes I. and M. Mellor, Uniaxial testing in rock mechanics laboratories., Eng. Geol., 1970, 4, 177-285
14. Heard H. C., Transition from brittle failure to ductile flow in Solehonfen limestone as a function of temperature, confining pressure, and interstial fluid pressure., In: Rock deformation., Griggs D., Handin J., Geol. Soc. Amer. Memoir 1960, 79, 193-226
15. Hudson J. A. and J. P. Harrison, Engineering rock mechanics. An introduction to the principles., Tarrytown, NY : Pergamon, 1997, 444p.

16. Jaeger J. C. and N. G. W Cook, Fundamentals of Rock mechanics., Chapman and Hall, London, 1979 585p

17. Karman von Theodore, Uber den Mechanismus des Widerstandes, den ein bewegter Körper in einer Flüssigkeit erfährt, 1911

18. Kim M. M. and H. Y. Ko, Multistage Triaxial Testing of Rocks., Geotechnical Testing 1979, 2, 98-105

19. Kovari K. and A. Tisa, Multiple failure state and strain controlled triaxial tests., Rock Mechanics, 1975, **7**, 17–33.

20. Kovari K., Tisa A., Einstein H. and J. A. Franklin, Suggested methods for determining the strength materials in triaxial compression., Int. J. Rock Mechanics Min. Sci. & Geomechanics Abstract, 1983, 20, 6, 283-290

21. Mogi K., Pressure dependence of rock strength and transition from brittle ductile flow. Bull. Earthquake Res. Inst. Tokyo Univ., 1966, 44, 215-232

22. Mogi K., Effects of the intermediate principal stress on rock failure., JGR, 1968, 72, 5117-5131

23. Orowan E., Mechanism of seismic faulting., Geol. Soc. Am. Mem.,1960, 79, 323-345

24. Paterson, M. S., Experimental Rock Deformation: The Brittle Field., Springer Verlag, New York, 1978, 254pp.

25. Scholz, C. H., Microfracturing and the inelastic deformation of rock in compression., J. Geophys. Res., 1968, 73, 1447-1454

26. Scholz, C. H., The Mechanics of earthquakes and Faulting., Cambridge University Press, New York, 1990, 439pp.

27. Sheorey, R. P, Empirical rock failure criteria., Rotterdam ; Brookfield , Vt. : A.A. Balkema, 1997, 175pp.

28. Sondergeld C. H. and C. S. Rai, A New Concept in Quantitative Core characterization., The Leading Edge, 1993, 774-779.

29. Standard test method for triaxial compressive strength of undrained rock core specimens without pore pressure measurements., 1980, ASTM D2664 – 80

30. Stanley C. J., A rapid accurate steady-state Klinkenberg permeameter., 1972, SPE 3535

31. Walsh J. B., The effects of cracks in rocks on Poisson's ratio., Geophys. Res., 1965, 70, 20, 5249-5258

32. Weidinger P., Blum W., Hunsche U. and Hamplel A, The influence of friction on plastic deformation in compression test., Phys. Stat. Sol. 1996, 156, 305-315

33. Wilhelmi B. and W. H. Somerton, Simultaneous measurement of pore and elastic properties of rocks under triaxial test conditions., J. Soc. Pet. Engrs. 1967, 7, 283-294

# APPENDIX I

***Stress-strain plots of single stage tests.***

Figure A1.1 Sample H20 tested uniaxially.

Figure AI.2 Sample H21 tested triaxially at 3.45 MPa confining pressure.

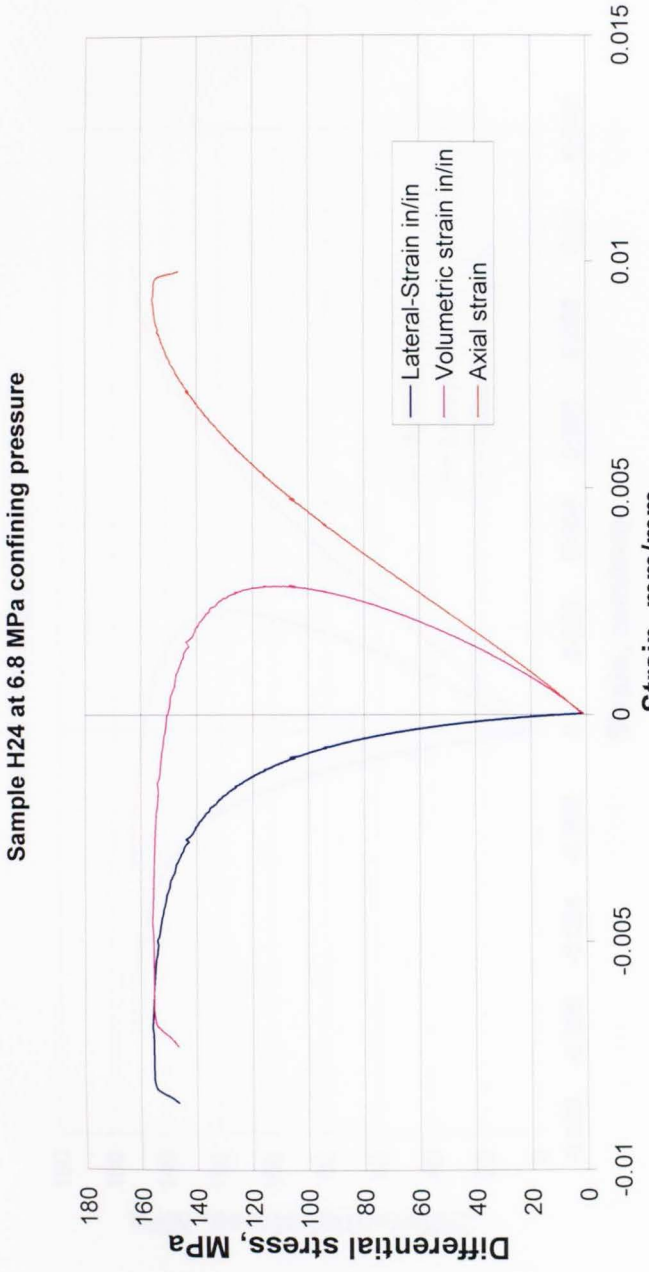


**Figure AI.3 Sample H24 tested triaxially at 6.8 MPa confining pressure.**

**Figure AI.4 Sample H5 tested triaxially at 17.24 MPa confining pressure.**

**Figure AI.5 Sample H9 tested triaxially at 24.14 MPa confining pressure.**

Figure AI.6 Sample H21 tested triaxially at 34.48 MPa confining pressure.

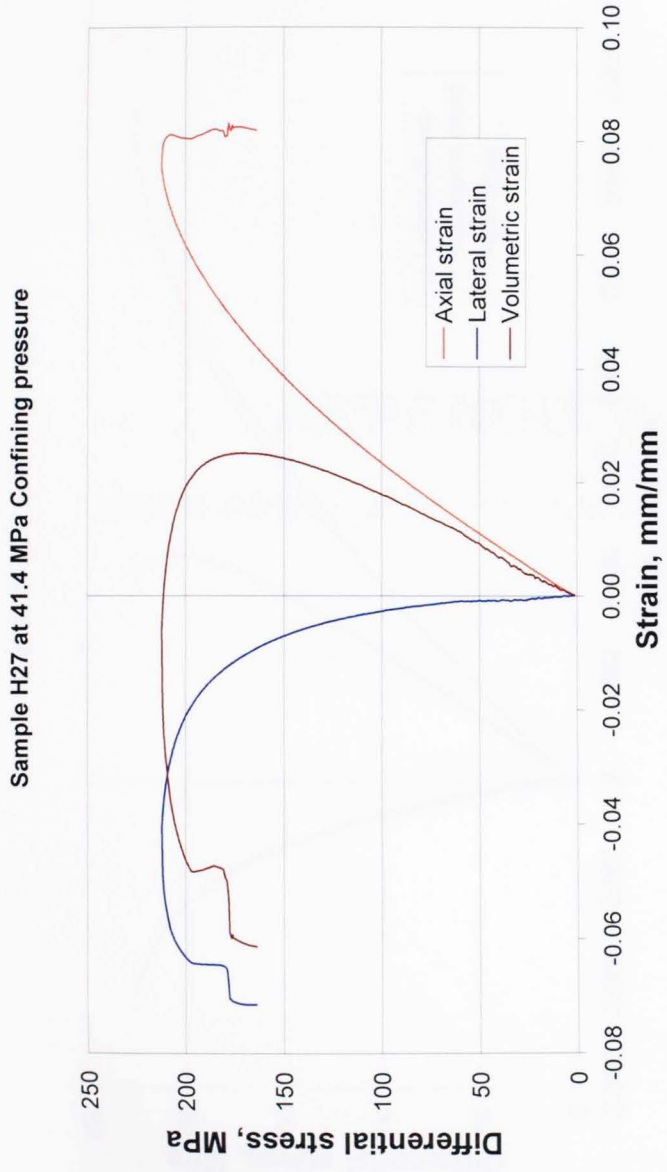


**Figure AI.7 Sample H27 tested triaxially at 41.4 MPa confining pressure.**

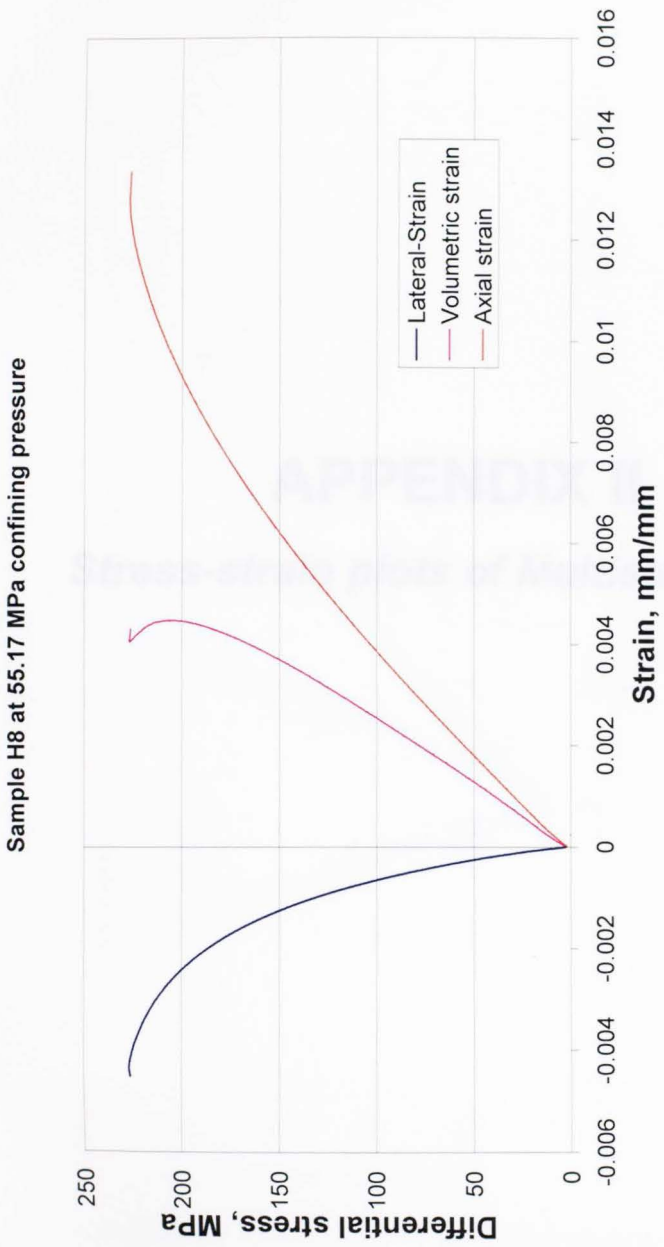


**Figure AI.8 Sample H8 tested triaxially at 55.17 MPa confining pressure.**

# APPENDIX II

## *Stress-strain plots of Multistage tests*

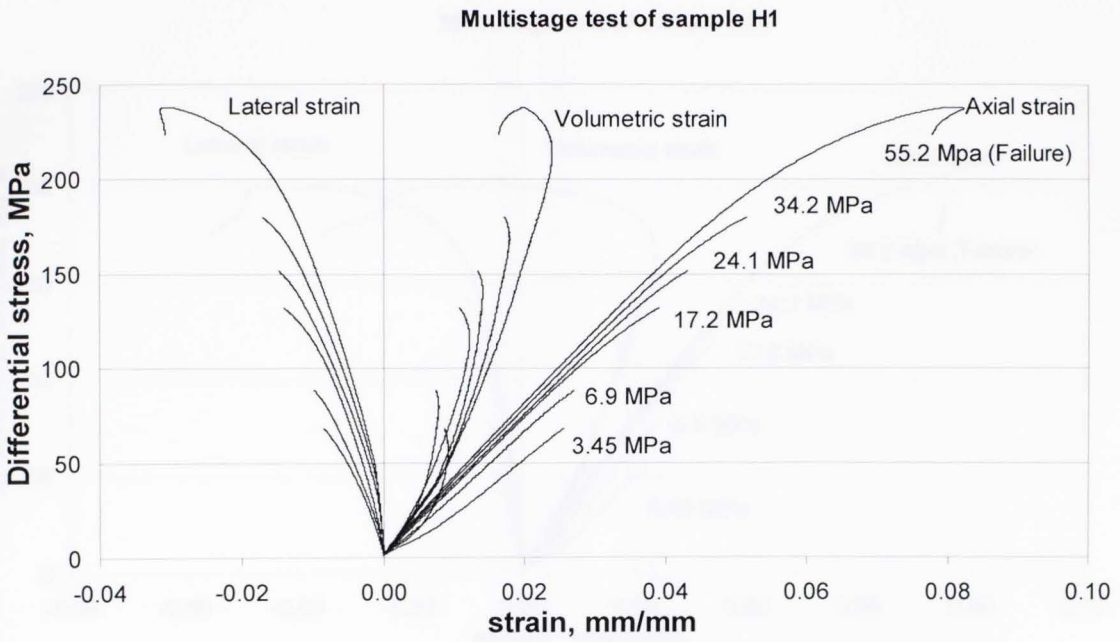


Figure AII.1 Sample H1 tested using multistage triaxial technique.

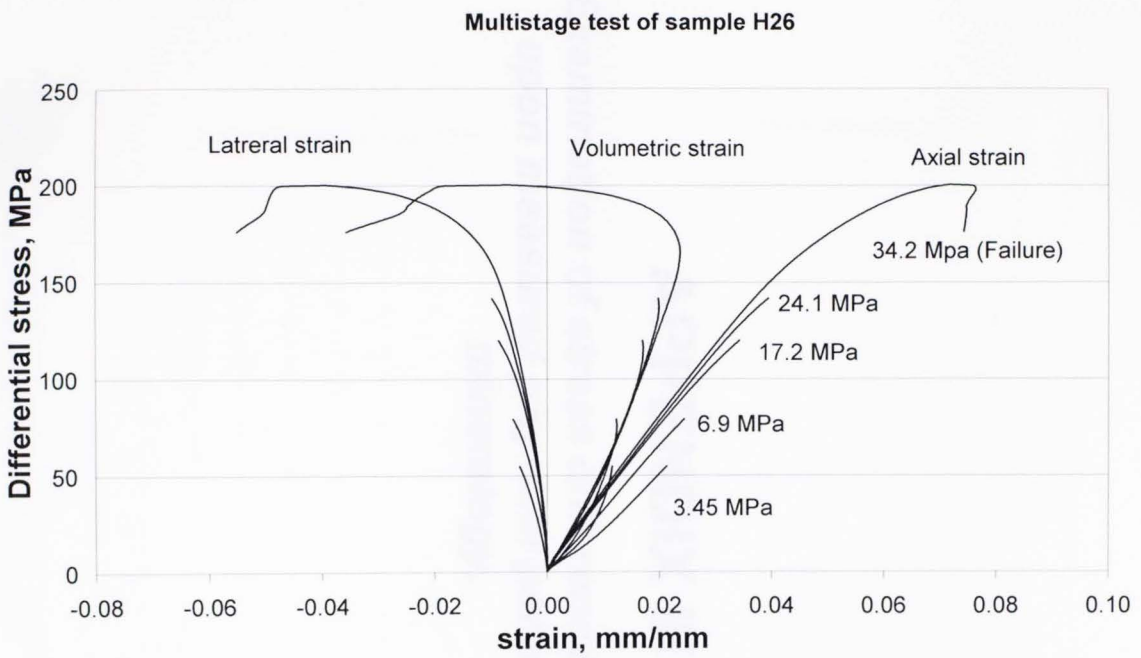


Figure AII.2 Sample H26 tested using multistage triaxial technique.

# APPENDIX III

***Examination of stress difference dependency upon measured physical parameters and mineralogy.***

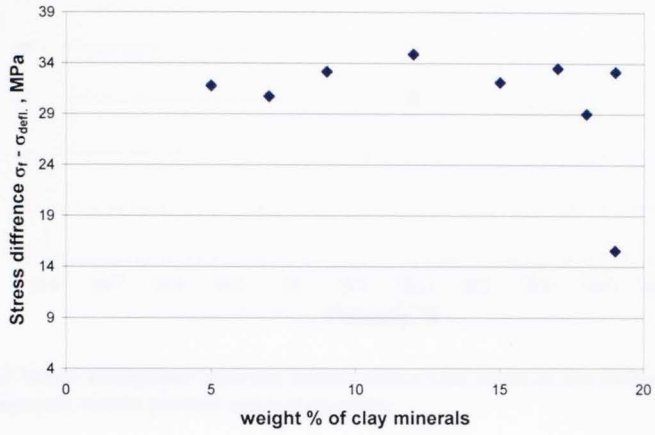


**Figure AIII.1 Stress difference between failure stress and stress at the deflection of the volumetric strain plotted against the percentage of total clay content.**

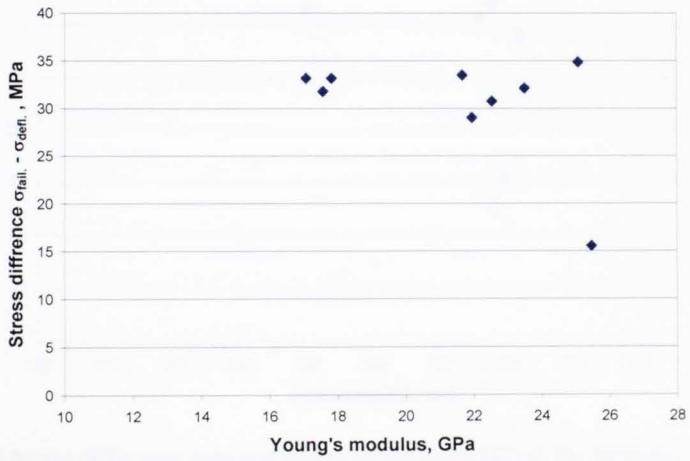


**Figure AIII.2 Stress difference between failure stress and stress at the deflection of the volumetric strain plotted against the Young's modulus.**

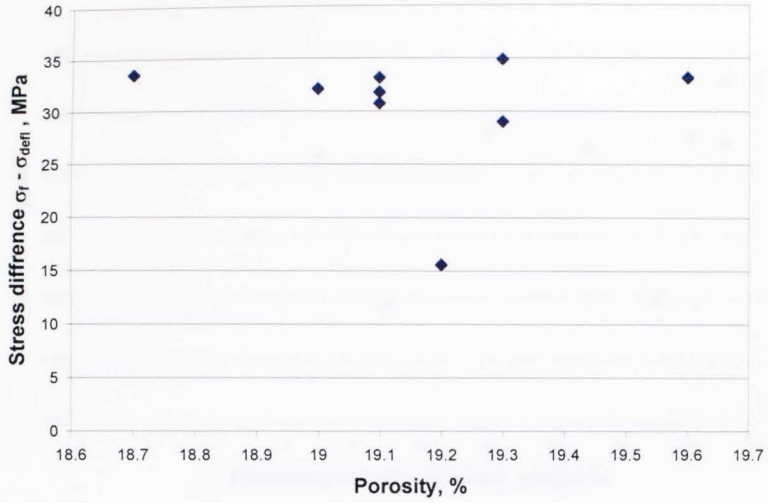


**Figure AIII.3 Stress difference between failure stress and stress at the deflection of the volumetric strain plotted against porosity.**

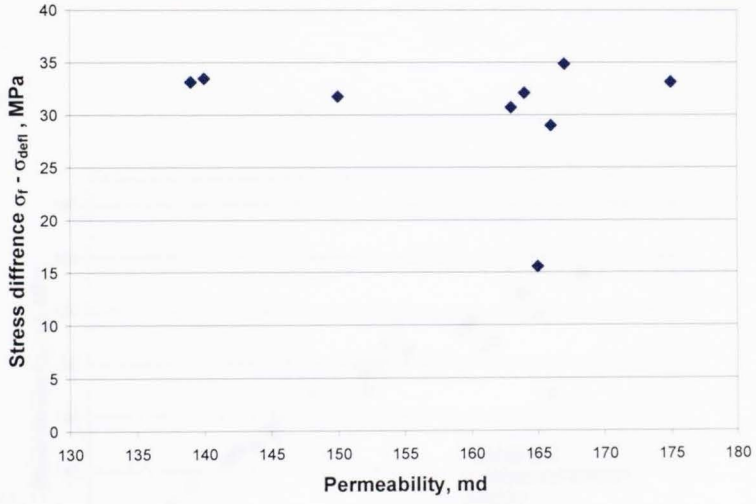


**Figure AIII.4 Stress difference between failure stress and stress at the deflection of the volumetric strain plotted against permeability.**

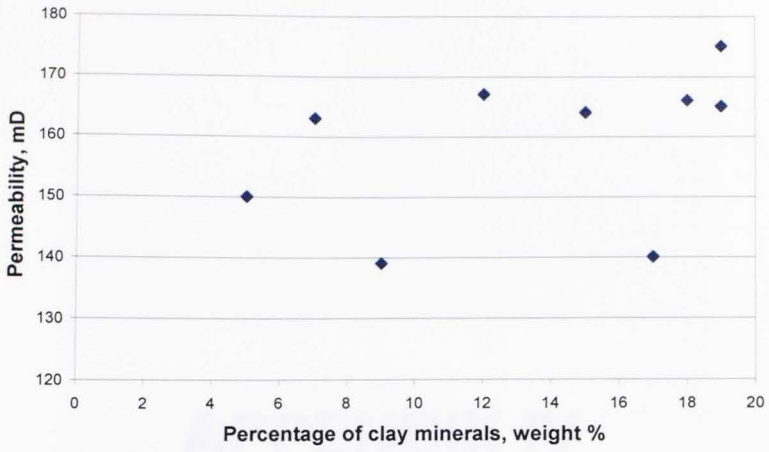


**Figure AIII.5 Permeability plotted against weight percentage of clay minerals.**

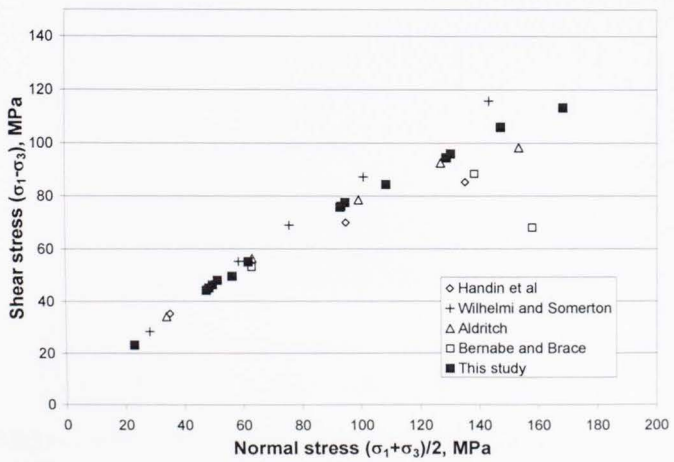


**Figure AIII.6 Plot of reported mechanical data results for Berea sandstone**

# APPENDIX IV

***Photographs of the failed samples***

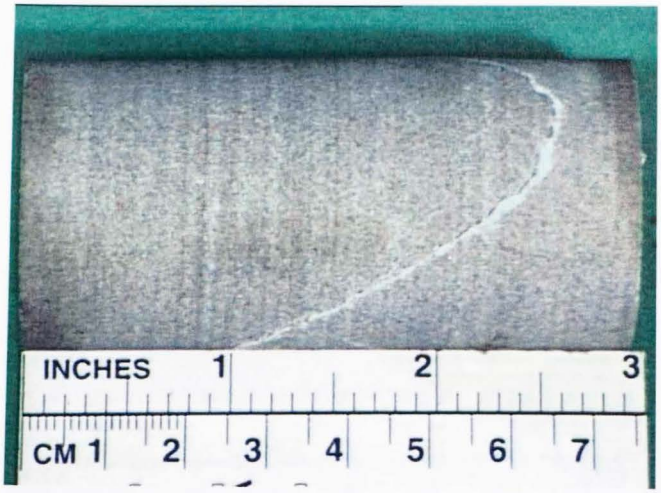


Figure AIV.1 Photograph of a multistage sample H16 after the completion of the test. (Porosity = 19.4%; k = 148 mD; $\beta = 60^{\circ}$).

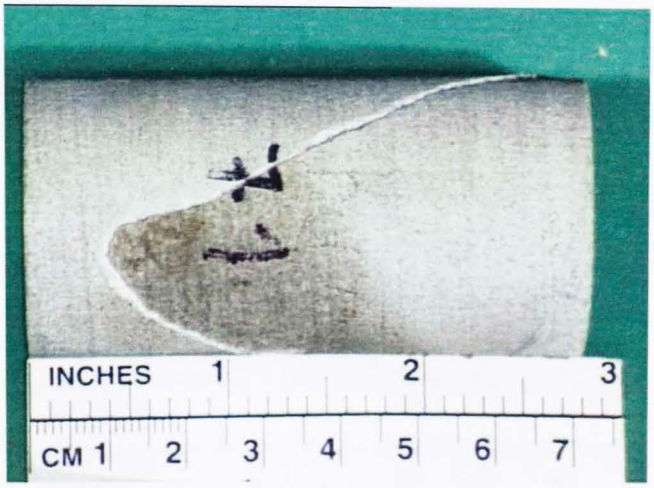


Figure AIV.2 Photograph showing the failure plane orientation for multistage sample H22. (Porosity = 18.6%; k = 101 mD; $\beta = 62^{\circ}$).

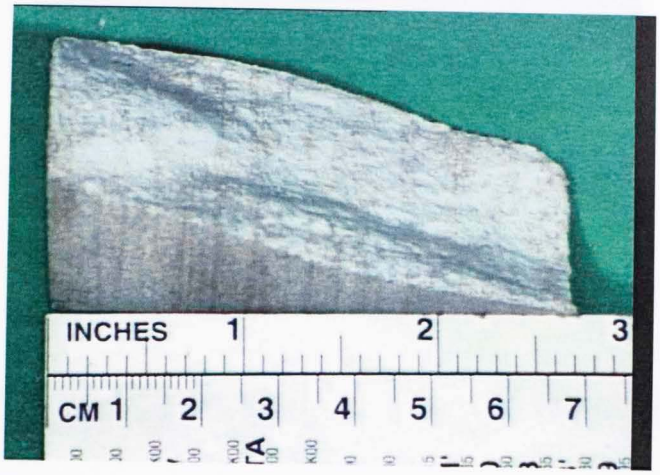


Figure AIV.3 Photograph of sample H23. Note the pressure cone that is formed at the bottom of the sample due to friction with the steel platens. ($\sigma_c$ = 17.24; $\sigma_{fail}$ = 172 MPa Porosity = 22%; k = 110 mD; $\beta = 65^{\circ}$).

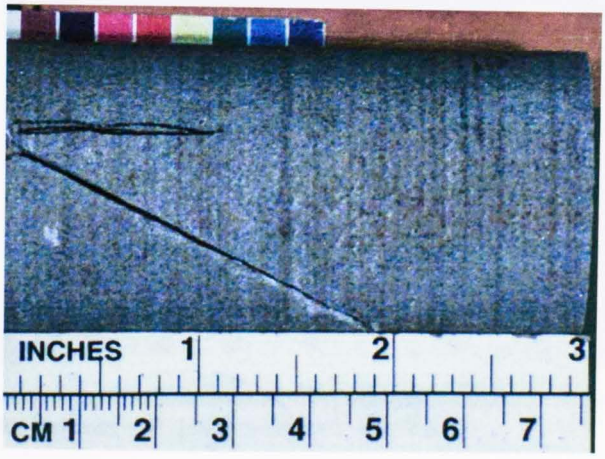


Figure AIV.4 Photograph of multistage sample H26. (Porosity = 19.1%; k = 200 mD; $\beta = 60^{\circ}$).

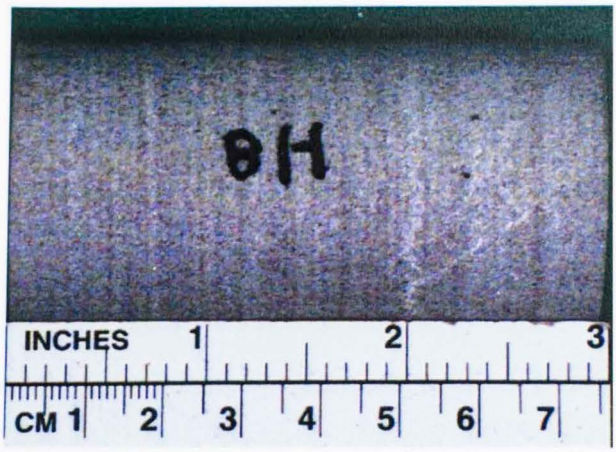


Figure AIV.5 Photograph of sample H8 ($\sigma_c$ = 55.17; $\sigma_{fail}$ = 281 MPa Porosity = 19.5%; k = 174 mD; $\beta = 55^0$).

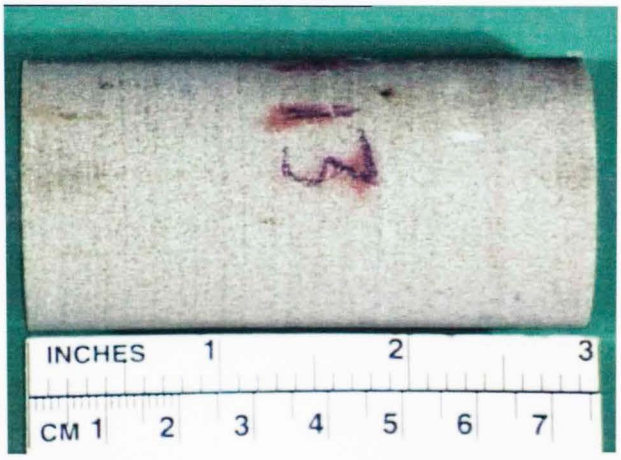


Figure AIV.6 Photograph of sample H13 showing ductile failure. ($\sigma_c$ = 3.45MPa; $\sigma_{fail}$ = 95.9 MPa Porosity = 19.1%; k = 150 mD; $\beta \approx 90^0$).

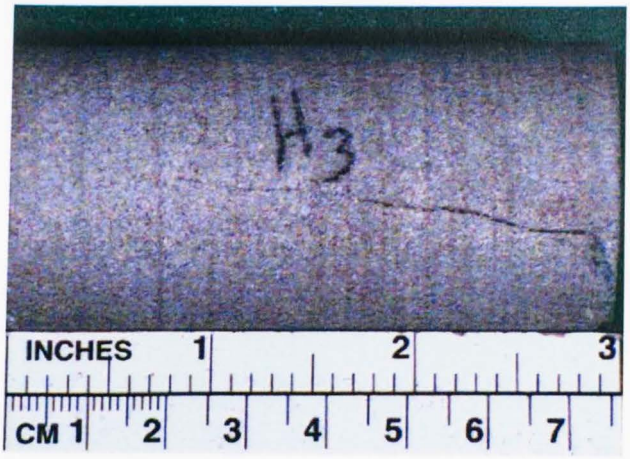


Figure AIV.7 Photograph of sample H3 broken at low confining pressure. ($\sigma_c$ = 3.45MPa; $\sigma_{fail}$ = 95.9 MPa Porosity = 19.1%; k = 150 mD; $\beta \approx 90^{o}$).